https://doi.org/10.5194/gmd-2021-385
Preprint. Discussion started: 3 December 2021

Geoscientific Model Development Discussions

Implementation of HONO into the chemistry-climate model CHASER (V4.0): roles in tropospheric chemistry

Phuc T. M. Ha[1], Yugo Kanaya[2], Fumikazu Taketani[2], Maria Dolores Andrés Hernández[3], Benjamin Schreiner[4], Klaus Pfeilsticker[4], Kengo Sudo[1,2]

[1] Graduate School of Environmental Studies, Nagoya University, Nagoya 464-8601, Japan
[2] Research Institute for Global Change, JAMSTEC, Yokohama 236-0001, Japan
[3] Institut für Umweltphysik, Universität Bremen, Otto-Hahn-Allee 1, Bremen 28359, Germany
[4] Institut für Umweltphysik (IUP), Universität Heidelberg, INF 229, Heidelberg 69120, Germany

Correspondence to: Phuc T. M. Ha (hathiminh.phuc@gmail.com)

Abstract. Nitrous acid (HONO) is an important atmospheric gas given its contribution to the cycles of NO_x and HO_x, but its role in global atmospheric photochemistry is not fully understood. This study, for the first time, implemented three pathways of HONO formation in the chemistry-climate model CHASER (MIROC-ESM) to explore three physical phenomena: gas-phase kinetic reactions (GRs), direct emission (EM), and heterogeneous reactions on cloud/aerosol particles (HRs). We evaluated the simulations by the atmospheric measurements from the OMI (Ozone Monitoring Instrument), EANET (Acid Deposition Monitoring Network in eastern Asia) / EMEP (European Monitoring and Evaluation Programme) ground-based stationary observations, observations from the ship *R/V Mirai*, and aircraft-based measurements by ATom1 (atmospheric tomography) and EMeRGe-Asia-2018 (Effect of Megacities on the Transport and Transformation of Pollutants on the Regional to Global scales). We showed that the inclusion of the HONO chemistry in the modeling process reduces the model bias against the measurements for $PM_{2.5}$, NO_3^-/HNO_3, NO_2, OH, O_3, and CO, especially in the lower troposphere and the North Pacific (NP) region.

We found that the retrieved global abundance of tropospheric HONO was 1.4 TgN. Of the three source pathways, HRs and EM contributed 63% and 26% to the net HONO production, respectively. We also observed that, reactions on the aerosol surfaces contributed larger amounts of HONO (51%) than those on the cloud surfaces (12%). The model exhibited significant negative biases for daytime HONO in the Asian off-coast region, compared with the airborne measurements by EMeRGe-Asia-2018, indicating the existence of unknown daytime HONO sources. Strengthening of aerosol uptake of NO_2 near surface and in the middle troposphere, cloud uptake, and direct HONO emission are all potential yet-unknown HONO sources. We also found that the simulated HONO abundance and its impact on NO_x-O_3 chemistry are sensitive to the yield of the heterogeneous conversion of NO_2 to HONO (vs. HNO_3).

Inclusion of HONO reduces global tropospheric NO_x ($NO + NO_2$) levels by 20.4%, thereby weakening the tropospheric oxidizing capacity, which in turn, increases CH_4 lifetime (13%) and CO abundance (8%). HRs on the surfaces of cloud particles, which have been neglected in previous modeling studies, are the main drivers of these impacts. This effect is

https://doi.org/10.5194/gmd-2021-385
Preprint. Discussion started: 3 December 2021

Geoscientific Model Development Discussions

particularly salient for the substantial reductions of levels of OH (40–67%) and O_3 (30–45%) in the NP region during summer given the significant reduction of NO_x level (50–95%). In contrast, HRs on aerosol surfaces in China (Beijing) enhances OH and O_3 winter mean levels by 600–1700% and 10–33%, respectively, with regards to their minima in winter. Overall, our findings suggest that a global model that does not consider HONO heterogeneous mechanisms (especially HRs on cloud particle surfaces) may erroneously predict the effect of HONO in remote areas and polluted regions.

1 Introduction

Nitrous acid (HONO) is an important atmospheric gas as it participates in the cycles of nitrogen oxides (NO_x = NO + NO_2) and radical chemistry (OH, HO_2, and RO_2) (Kanaya et al., 2007; Ren et al., 2013; Whalley et al., 2018). Researchers have suggested to include the HONO chemistry in atmospheric chemistry models for more accurate simulations of oxidative substances (Jacob, 2000; Li et al., 2011). Despite the empirical evidences have indicated that the HONO concentrations in urban environments can reach 14 ppbv at night and can reach several hundred pptv throughout the day (Appel et al., 1990; Febo et al., 1996; Kanaya et al., 2007; Lee et al., 2016; Tan et al., 2017; Whalley et al., 2018), the HONO formation mechanism remains unclear. More specifically, the mechanisms of the HONO daytime sources have recently attracted considerable attention of researchers (Kleffmann et al., 2003; Li et al., 2014; VandenBoer et al., 2013; Xue et al., 2021a,b; Ye et al., 2018).

The only homogeneous reaction known to produce HONO in the troposphere is the direct combination of OH and NO (R2). Note that the major loss of HONO occurs via photolysis (R1) in the atmosphere at 300–405 nm:

(R1) HONO + $h\nu$ → OH + NO (300 nm < λ< 405 nm).

(R2) NO + OH + M → HONO + M

(R3) HONO + OH → NO_2 + H_2O

Moreover, the photolysis of HONO (R1) has attracted considerable attention in the literature as a critical source of OH radicals in the polluted urban atmosphere (e.g., Calvert et al., 1994; Harris et al., 1982; Jenkin et al., 1988; Platt and Perner, 1980). The OH level at sunrise can be increased by a factor of 5 due to the photolysis of HONO, with the regional daily maximum O_3 level increasing by 8% (Jenkin et al., 1988). Besides the direct loss via photolysis, the reaction of HONO with OH (R3) may also contribute to the daytime loss of HONO (Burkholder et al., 1992).

Notably, some night-time measurements hinted on the heterogeneous sources of HONO from aerosol surfaces. For instance, Harrison and Kitto (1994) have provided evidence about the HONO source from high concentration episodes of > 10 ppbv NO_2 for grassland in eastern England (Harrison and Kitto, 1994). Two reactions have been widely suggested to produce HONO on aerosol surfaces: $2NO_2 + H_2O$ → HONO + HNO_3 and NO + NO_2 + H_2O → 2HONO. The first process has been proven to be first-order with NO_2 and H_2O in reaction chamber studies (Sakamaki et al., 1983, Jenkin et al., 1988). The second process was evaluated by using laboratory surfaces (Sakamaki et al., 1983, Jenkin et al., 1988) and by using field observations in the presence of high O_3 and when NO_2 was the dominant form of NO_x (Kessler and Platt, 1984). As a result, the second process was proposed as a peculiarly important source of HONO in the urban atmosphere (Ammann et al., 1998;

https://doi.org/10.5194/gmd-2021-385
Preprint. Discussion started: 3 December 2021

Geoscientific Model Development Discussions

Gerecke et al., 1998). In the past two decades, researchers have investigated the heterogeneous NO_2 reactivity on vegetated, aqueous, sea salt, carbonaceous, and soot surfaces (Acker et al., 2001, 2006; Arens et al., 2001; Kleffmann and Wiesen, 2005; Kleffmann et al.,1998; Lammel and Cape, 1996; Lee et al., 2016; Notholt et al., 1992; Reisinger, 2000; Rubio et al., 2002; Stutz et al., 2002). In our model, these two processes are simplified as $NO_2 \rightarrow 0.5\ HONO + 0.5\ HNO_3$ (R4) and $NO_2 \rightarrow HONO$ (R5).

Also, some modeling studies have reported overestimations of HONO over remote areas, indicating the HONO release from or deposition in snow (Chu et al., 2000; Fenter and Rossi, 1996; Kerbrat et al., 2010), partitioning to cloud water (Bongartz et al. 1994; Cape et al., 1992; Harrison and Collins, 1998; Mertes and Wahner, 1995), and deliquescent aerosol surfaces (Harrison and Collins, 1998). The loss process occurs via the reaction $HONO + H_2O \rightarrow NO^- + H_3O^+$, simplified in our model as $HONO \rightarrow NO$ (R6) for surfaces of liquid and aqueous sulfate aerosols.

The natural sources of HONO include plant-foliar cuticles or soil biological crust (Hayashi and Noguchi, 2006; Oswald et al., 2013; Porada et al., 2019; Su et al., 2011), with estimated global total emission of 0.69 Tg yr^{-1} HONO–N (Porada et al., 2019). Given the widespread occurrence of nitrite-fertilized soil in natural environment, highly acidic soils are arguably the strong sources of HONO and OH (Su et al., 2011). This potentially important source has been likely overseen by many previous modeling studies at both global and regional scales. Soil emissions could sustain the daytime HONO budget at relatively low aerosol concentrations (Lu et al., 2018). Anthropogenic activities can also directly emit HONO through incomplete combustion, as vehicles, for instance, can yield as high concentrations as 7 ppb (Kirchstetter et al., 1996; Kurtenbach et al., 2001). In regional air quality models, HONO sources from vehicles and vessels are often given at 0.8–2.3% of NO_x emissions level, given the differences between gasoline and diesel vehicle types (e.g., Aumont et al., 2003; Kurtenbach et al., 2001; Li et al., 2011; Zhang et al., 2016). Many scholars have scrupulously addressed the effects of HONO in polluted regions as well. For instance, HONO-induced enhancements in winter daytime HO_x (up to >200% for OH) and O_3 (6–12%) over urban sites in China have been reported (Li et al., 2011; Lu et al., 2018; Zhang et al., 2016). However, another global modeling study suggested that O_3 levels are enhanced in response to additional OH production from the HONO photolysis only in high-NO_x regions, despite they can be decreased in some areas under low NOx conditions (Jorba et al., 2012). At the same time, another 3D modeling study used a constant occurrence ratio for HONO as 0.02 of NO_x and reported similar patterns for O_3 changes regarding HONO chemistry (Elshorbany et al., 2012). The NO_x reduction effects that follow the NO_2 conversion are suggested to be more critical over the oceans than over continental regions, with up to 20% NO_x reduction and 5%–20% HNO_3 enhancement over ocean regions of the lower troposphere (Martin et al., 2003).

As H_2O is required for the uptake of NO_2 on surfaces, wet surfaces have been broadly recommended as favored surfaces for NO_2 uptake. Therefore, cloud droplets can be an important surface for heterogeneous reactions of NO_2 because they are ubiquitous in the troposphere. Heterogeneous reactions by clouds can have a similar impact as aerosol particles on tropospheric O_3 and OH levels (Christopher et al., 2019). However, this aspect has been overlooked many times in previous studies, thereby, leading to potential underestimation (or even dismissing) of the potential effects over remote environments.

https://doi.org/10.5194/gmd-2021-385
Preprint. Discussion started: 3 December 2021


Geoscientific Model Development Discussions

In this study, we introduce the HONO chemistry into the global atmospheric chemistry model CHASER-V4.0 for the first time. The main idea for the HONO inclusion is to elaborate the model simulation for tropospheric oxidative substances, while focusing on aerosol and cloud processes. The model includes the detailed online calculation of O_3-HO_x-NO_x-CH_4-CO coupling and oxidation of non-methane hydrocarbons (NMHCs) (Sudo et al., 2002) and heterogeneous processes for N_2O_5, HO_2, and RO_2 radicals (Ha et al., 2021; Sekiya and Sudo, 2014; Sekiya et al., 2018; Sudo and Akimoto, 2007). In Section 2, we describe the approach, including the model description and configuration. In Section 3.1, our model is evaluated by the available observations for atmospheric species, including observations from satellites, ground stations, and ship/aircraft, particularly addressing the roles of the HRs. In addition, simulated daytime HONO was verified with aircraft measurements for an Asian off-coast region. Section 3.2 presents the model results for HONO distributions and global HONO impacts, including separate effects from each pathway. Finally, Section 4 effectively represents the summary and concluding remarks.

2 Method and configurations

2.1 Global chemistry model

This study applied the global chemistry model CHASER (MIROC-ESM) (Sudo et al., 2002, 2007; Watanabe et al., 2011), which considers the detailed photochemistry in the troposphere and stratosphere. The chemistry component of the model, based on CHASER-V4.0, retrieves the concentrations of 95 chemical species and 262 chemical reactions (58 photolytic, 183 kinetic, and 21 heterogeneous reactions on polar stratospheric clouds), including the new HONO chemistry implemented in this study. We used the HTAP-II (Hemispheric Transport of Air Pollution) emission inventory for 2008 (https://edgar.jrc.ec.europa.eu/dataset_htap_v2, last access: 16th, Nov 2021) for O_3 and aerosol precursors (NO_x, CO, VOCs, SO_2), with biomass burning emissions derived from the MACC (Monitoring Atmospheric Composition and Climate) reanalysis system (https://gmao.gsfc.nasa.gov/reanalysis/MERRA/ceop.php). The details about the CHASER can be found in the earlier studies (Ha et al., 2021; Morgenstern et al., 2017; Sekiya et al., 2018). In this study, the newly added HONO system includes three pathways of HONO formation and interactions: (1) gas phase formation via the NO + OH reaction (R2), the photolysis of HONO (R1), and the reaction of HONO with OH (R3), hereafter denoted as GRs; (2) HONO direct emissions estimated from anthropogenic- and soil-NO_x emissions (hereafter denoted as EM); and (3) the HONO conversion from NO_2 (R4, R5) and its loss on liquid/ice surfaces and aqueous aerosols (R6), which is hereafter denoted as HRs.

2.2 Experimental setup

The Global Emissions Initiative (GEIA) inventory (http://www.geiacenter.org/) is applied to quantify the soil NOx emissions (6 TgN yr^{-1}) and anthropogenic NO_x emissions (45 Tg N yr^{-1}). Since this broadly applied inventory is not currently available for HONO, this study tentatively imposes the HONO direct emissions based on the above NO_x emission inventory through a constant factor of 0.1 (10% of NO_x emissions). This assumption (soils + combustion) leads to a global HONO soil-emission estimate of about 0.6 TgN yr^{-1}, which is equivalent to the estimate from Porada et al. (2019), and it suggests that the

https://doi.org/10.5194/gmd-2021-385
Preprint. Discussion started: 3 December 2021

Geoscientific Model Development Discussions

anthropogenic emissions for HONO is 4.5 TgN yr^{-1}. For HONO from exhaust sources, this factor (10%) is considerably higher than the previously reported estimate of 0.7%, derived for combustion (Xue et al., 2021b) or 0.8–2.3% for on-road vehicles (Aumont et al., 2003; Kurtenbach et al., 2001; Li et al., 2011) and 3%–6% for commercial aircraft (Lee et al., 2011). This factor intends to show the apparent potential impacts of direct HONO sources on the troposphere.

Table 1: Computation packages in the chemistry-climate model "CHASER"

Base model	MIROC4.5 AGCM
Spatial resolution	Horizontal, T42 (2.8° × 2.8°); vertical, 36 layers (surfaces approx. 50 km)
Meteorology (u, v, T)	Nudged to the NCEP2 FNL reanalysis
Emission (anthropogenic, natural)	Industry traffic, Vegetation Ocean Biomass burning specified by MACC reanalysis
Aerosol	BC/OC, sea-salt, and dust BC ageing with SO_x/SOA production
Chemical process	94 chemical species, 263 chemical reactions (gas phase, liquid phase, non-uniform O_x-NO_x-HO_x-CH_4-CO chemistry with VOCs SO_2, DMS oxidation (sulfate aerosol simulation) SO_4-NO_3-NH_4 system and nitrate formation Formation of SOA BC ageing (+) Heterogeneous reactions: 8 reactions of N_2O_5, HO_2, RO_2; constant uptake coefficients (γ) on types of aerosols (Ice, Liquid, Sulfate, Sea salt, Dust, OC)

The photolysis reaction of HONO (R1) is employed with the wavelength-dependent cross-sections following the recent study of Burkholder et al. (2015).

The kinetic of homogeneous reactions NO + OH + M → HONO + M (R2) and HONO + OH → NO_2 + H_2O (R3) is applied with the low and high-pressure-limit rate constants, which are temperature dependent, as suggested in the aforementioned study.

In CHASER, the heterogeneous chemistry of interest is simplified as a first-order chemical loss in the aerosol phase for a species transferred from the gas phase. The rate of this pseudo loss is combined, and the first-order-loss rate for heterogeneous processes is calculated by using the Schwartz theory (Jacob, 2000; Schwartz, 1986), being simply treated with the mass transfer limitations in addition to the reactive uptake coefficient (γ) (Ha et al., 2021). Note that in CHASER, only surface reactions are considered, and there is no bulk particle reaction for the HR scheme.

The uptake coefficient parameter (γ) is defined as the net probability that a molecule X undergoing a gas-kinetic collision with a surface is taken up onto the surface. An average uptake coefficient for NO_2 (R4) of 10^{-4} (10^{-6}–10^{-3}) for the conversion of aqueous aerosols and clouds has been previously suggested (Jacob, 2000; Kleffmann et al., 1998; Li et al., 2018; Lu et al.,

https://doi.org/10.5194/gmd-2021-385
Preprint. Discussion started: 3 December 2021

Geoscientific Model Development Discussions

2018). The NO_2 uptake by organic carbon aerosols has been reported to have similar coefficient values (Salgado-Muñoz and Rossi, 2002). The uptake coefficient for fresh black carbon is highly efficient and equals 3×10^{-3} (Ammann et al., 1998; Li et al., 2018). The parameters for the uptake coefficients of R4 applied in the CHASER model are shown in Table 2.

As previous studies have noted, the fast initial uptake of NO_2 is observed on soot with an uptake coefficient in the range of 10^{-1}–10^{-4} (Ammann et al., 1996, 1998). However, it rapidly decreased to ~10^{-7} over 5 min (Kleffmann et al., 1999) to < 4×10^{-8} for 5-day aged surfaces (Saathoff et al., 2001). In organic soot, γ is in the range of 10^{-4}–10^{-6} (Al-Abadleh et al., 2000; Ammann et al., 1996; Arens et al., 2001; Salgado-Muñoz et al., 2002). In CHASER, the NO_2 conversion on organic carbon and soot (R5) was tentatively applied with uptake coefficients of 10^{-4} and 3×10^{-4}, respectively, which also falls within the previously suggested range (10^{-6}–10^{-3}) considering the higher efficiency for soot (Table 2).

Also, previous laboratory experiments have introduced a wide range for the uptake coefficient of HONO by (R6), that is, 3.7×10^{-3} at 178 K to 1.3×10^{-5} at 200 K for the ice surface (Fenter and Rossi, 1996; Chu et al., 2000) and 4×10^{-3}–4×10^{-2} at 278 K (Mertes and Wahner, 1995) or 0.03 × 0.15 at 297 K (Bongartz et al. 1994) for liquid water surfaces. In the aerosol flow reactor experiment on deliquescent sodium chloride and ammonium sulfate droplets at 279 K, the HONO reactive uptake coefficient of 0.0028 for 85% relative humidity has been previously obtained (Harrison and Collins, 1998). In CHASER, the aforementioned reference values for HONO uptake on ice, liquid clouds, and aqueous sulfate are simply averaged to be used as a heterogeneous loss of HONO (R6) in atmosphere (Table 2: last row).

Table 2: Uptake coefficients for heterogeneous formation and loss of HONO

		γ_{ice}	$\gamma_{liq.}$	$\gamma_{sulf.}$	γ_{salt}	γ_{dust}	γ_{oc}	γ_{ec}
R4	NO_2 → 0.5HONO + 0.5HNO_3	0.0	0.0001	0.0001	0.0001	0.0001	0.0001	0.003
R5	NO_2 → HONO	0.0	0.0	0.0	0.0	0.0	0.0001	0.0003
R6	HONO → NO	0.002	0.03	0.003	0.0	0.0	0.0	0.0

2.3 Simulations

In this study, two main simulations, OLD and STD, and three sensitivity simulations (Table 3, no. 2–4) were conducted to isolate the distinct impacts of each pathway of the HONO chemistry for different surface types considered in the model (Table 3). The OLD simulation is run with the base model configuration without any HONO chemistry (see more details about the OLD case in Ha et al., 2021), whereas the control case (STD) considers all three types of HONO sources: direct emissions (EM), gas-phase reactions (GRs), and heterogeneous reactions (HRs). To quantify the effects of each mechanism using Eq. (1), two sensitivity cases (GR, GR+HR) intentionally implement GRs (R1, R2, R3) into the OLD case and HRs (R1, R2, R3, R4, R5, R6) into the GR case, respectively. GR+HR (cld) is another sensitive case like GR+HR, with HRs on aerosols excluded to investigate the different effects of clouds and aerosols. Eq. (1) determines the effects of each mechanism on atmospheric

https://doi.org/10.5194/gmd-2021-385
Preprint. Discussion started: 3 December 2021


Geoscientific Model Development Discussions

species i (i = OH, O_3, NO_x, CO) by concentration differences of i in two relevant cases being compared to that in the OLD case.

$$E_i = \frac{(Case1_i - Case2_i)}{OLD_i} * 100\ (\%), \quad (1)$$

where $Case1_i$ and $Case2_i$ are the concentrations of i in two separate cases: GR and OLD cases for the pure effects by the gaseous mechanism; GR+HR and GR cases for the effects of heterogeneous mechanisms; STD and GR+HR cases for the HONO emissions effects; and GR+HR(cld) and GR cases for the effects of heterogeneous reactions that exclusively occur on ice and cloud particles.

Table 3: Sensitivity simulations in this work.

No.	Simulation ID	HRs (HONO)		GRs (HONO)	EM (HONO)
		clouds	aerosols		
1	OLD				
2	GR			×	
3	GR+HR(cld)	×		×	
4	GR+HR	×	×	×	
5	STD	×	×	×	×

2.4 Observation data for model evaluation

We evaluated the OLD, STD, and sensitivity simulations with ground-based, ship-based, aircraft, and satellite measurements. The observational information and locations of the surface site and ship/aircraft tracks for the observations used in this study are summarized in Table 4, Figure 1, Figure 4, and Figure S5.

Simulated tropospheric column ozone was also evaluated by using tropospheric column O_3 (TCO) derived from the OMI (Ozone Monitoring Instrument) spaceborne observations (https://daac.gsfc.nasa.gov/). To this end, the monthly data from 45 stations during 2010–2016 were used to verify aerosol surface concentrations (sulfate, nitrate) and trace gases (HNO_3, NO_x, O_3) in the Acid Deposition Monitoring Network in eastern Asia (EANET: https://www.eanet.asia/). We also used the European Monitoring and Evaluation Programme (EMEP: https://www.emep.int/) data, which compiles observations over 245 European stations. We also utilized the ship-based observational data from the *R/V Mirai* cruise (http://www.jamstec.go.jp/e/about/equipment/ships/mirai.html) undertaken by the Japan Agency for Marine-Earth Science and Technology (JAMSTEC). This study uses the surface CO and O_3 concentration data from the summers of 2015–2017 along the Japan-Alaska routes. The model data were compiled in the hourly timestep and interpolated, corresponding to the *Mirai* time step and coordinates. To verify the vertical tropospheric profiles, ATom1 aircraft measurements (https://espo.nasa.gov/atom/content/ATom) for NO_2, OH, CO, and O_3 were employed.

Daytime HONO concentrations were also analyzed by using the DLR-HALO aircraft (Operator Deutsches Zentrum für Luft- und Raumfahrt - High-Altitude and Long-Range research aircraft) measurements made during the EMeRGe-Asia (Effect of Megacities on the Transport and Transformation of Pollutants on the Regional to Global scales) campaign in March and

https://doi.org/10.5194/gmd-2021-385
Preprint. Discussion started: 3 December 2021

Geoscientific Model Development Discussions

April 2018, over an off-coast region between Korea (including the Jeju Island as the part of the domain), Taiwan, and the Philippines (http://www.iup.uni-bremen.de/emerge/home/). The measuring time falls in the range of 0:00 UTC to 9:00 UTC, around 8:00 to 17:00 in local time (UTC+8). Verification with EMeRGe data helps to explore the daytime HONO chemistry mechanisms in the free troposphere.

A model bias for each species was calculated as the difference between the simulated and observed concentrations, as shown in Eq. (2), where N is the total number of data points used in the calculation.

$$bias = \frac{\sum_1^N Model - Observation}{N} \quad (2)$$

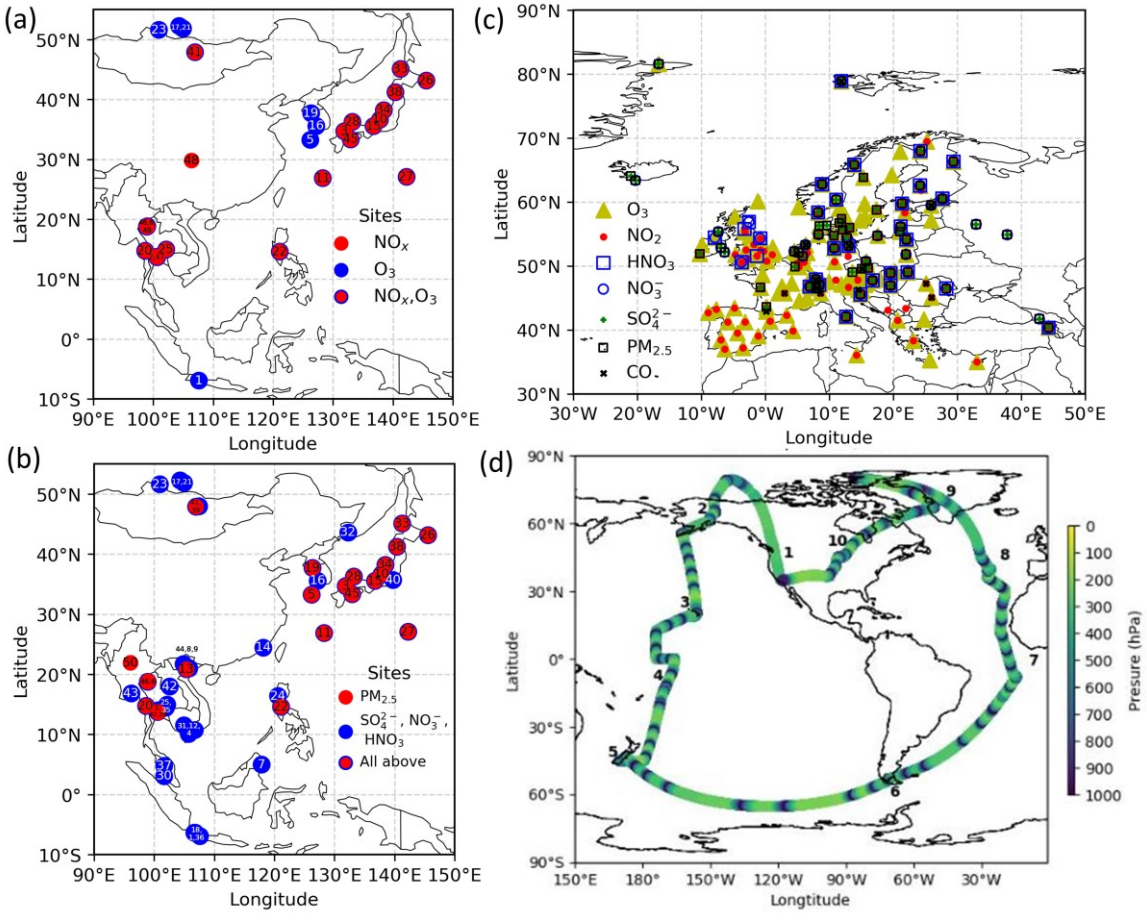

Figure 1: Location of measurements. (a) EANET stations for NO_x and O_3 and (b) for $PM_{2.5}$, SO_4^2, NO_3^-, and HNO_3, (c) EMEP stations, and (d) ATom1 cruising altitudes are plotted. In (a) and (b), each number described station name (see Table S1). In (d), numbers show flight tracks.

Table 4: Lists of the datasets used in this study for verification. Related simulations with their original model timestep are interpolated to the comparing timestep.

Verified species	Regions	Dataset name	Time	Measuring step	Model step	Interpolating step

https://doi.org/10.5194/gmd-2021-385
Preprint. Discussion started: 3 December 2021

Geoscientific Model Development Discussions

$PM_{2.5}$, SO_4^{2-}, NO_3^-, NO_x, O_3, HNO_3	East Asia	EANET (station)	2010–2016	Daily to 2-weekly	Daily	Monthly
$PM_{2.5}$, SO_4^{2-}, NO_3^-, NO_x, O_3, CO	Europe	EMEP (station)	2010–2016	Hourly	Daily	Monthly
CO, O_3	Australia – Indonesia – Japan – Alaska	*Mirai* (vessel)	8,9/2015 1,8,9/2016 7,8,9/2017	30 min	1 h	30 min
NO_2, OH, CO, O_3	Pacific, Atlantic ocean, Greenland, North America	ATom1 (aircraft)	8/2016	30 min	1 h	30 min
TCO	60°S - 60°N	OMI (Satellite)	2010–2016	Daily	Daily	Monthly
HONO	Jeju-Korea, Taiwan, and Philippine	EMeRGe (aircraft)	17/3/2018–4/4/2018	15–30 s	Hourly	14–30 s

3 Results and Discussion

3.1 Model verifications for cloud fraction, surface aerosol density, atmospheric species, and effects on HONO mechanisms

3.1.1 Verification for cloud fraction, surface aerosol density, and tropospheric column ozone

In this study, besides the conversion of NO_2 onto clouds and aqueous particles (R4), the losses of HONO onto ice and liquid clouds were also included (R6). Therefore, for accurate simulations of HRs, we need to examine the cloud distribution. The CHASER model applies the common cloud maximum-random overlap assumptions (MRAN) in the radiation and cloud microphysics schemes as other general circulation models to estimate the distribution of the cloud fraction. The verification by using the satellite observation data ISCCP D2, CALIPSO-GOCCP, and reanalysis data JRA55 generally revealed good correlation, whereas notable (10–20%) underestimation for the entire troposphere was yet salient. During June – July – August (JJA), CHASER's cloud fraction is likely overestimated for the lower troposphere of the North Pacific (NP) region (10–20% compared to JRA55 reanalysis data). This finding indicates that thorough scrutiny of any impacts in this region is highly required (see the discussion in Section 3.2). Note that more detailed information for cloud verification for CHASER has been provided by Ha et al. (2021).

The heterogeneous processes by clouds and aerosol particles are parameterized by using surface aerosol density (SAD) estimations alongside the cloud fraction and aerosol concentration. During DJF, the simulated total SAD is attributed to all types of aerosols. However, for JJA, liquid clouds and sulfate aerosols are the principal SAD sources. This is peculiarly visible pattern for the northern polar and mid-latitude maritime regions. The performance for aerosol SAD in our model is in line with the earlier report by Thornton et al., (2008), except for sea salt density, which was very low in our model (up to 2 $\mu m^2\ cm^{-3}$) compared to their work (up to 75 $\mu m^2\ cm^{-3}$). This disagreement may be ascribed to the different size distributions for sea salt in the two models. The distribution of SAD is discussed in more detail in an earlier report (Ha et al., 2021).

https://doi.org/10.5194/gmd-2021-385
Preprint. Discussion started: 3 December 2021

Geoscientific Model Development Discussions

The STD run with HONO improves the overall tropospheric column ozone (TCO) distribution observed by the OMI, especially at the mid-latitudes. Figure 2 shows that the O_3-reducing effects of HONO chemistry greatly reduced the model overestimates in the OLD simulation for the general Northern Hemisphere and polluted regions such as China. However, in the NP region, the inclusion of HONO only reduces the model overestimates during the insignificant episodes of TCO (autumn to early winter) while extending the underestimates for TCO for the rest of the year (Figure S3(b)). These O_3 underestimates in the NP region are also visible for the modeled surface air versus the measurements during the *Mirai* cruises (Figure 4(a,b)). Notably, these underestimates for O_3 could hold up to 400 hPa, as seen in comparison with the ATom1 flights (Figure 7(f): 400–900 hPa). This phenomenon can be related to the stratospheric downward transport and insufficient vertical mixing, as discussed in Sections 3.1.3 and 3.1.4, for comparisons in the NP region's surface air and free troposphere. Although the HONO level in STD remains < 10 ppt for this area (Figure 10), the O_3 reducing effects exacerbate the model discrepancy. The HONO photochemistry is unlikely to be the main driver of this phenomenon as the ozone simulation is improved over the continents when the HONO photochemistry is included.

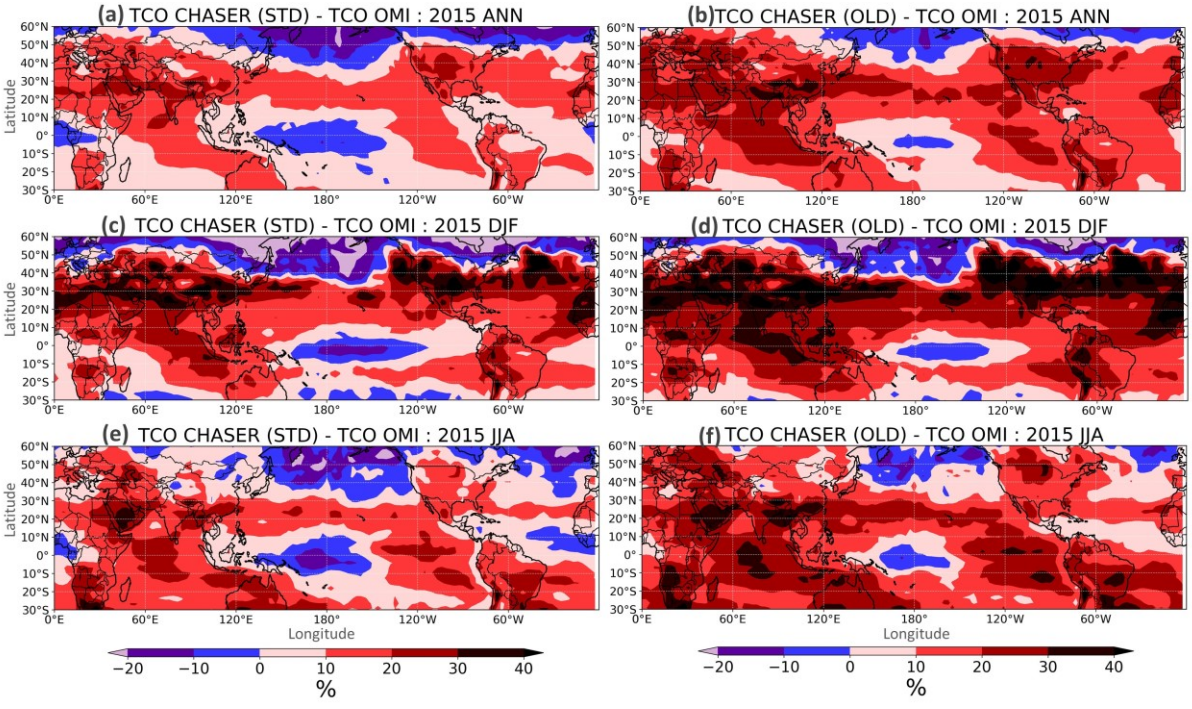

Figure 2: TCO percentage differences between model and OMI. Left panels show STD versus OMI; right panels show OLD versus OMI for annual (a,b), December – January – February (c,d), June – July – August (e,f). Black boxes indicate the NP region; dash boxes indicate the Chinese region.

3.1.2 Effects of HONO chemistry in the continental near-surface layer

The effects of HONO chemistry in the continental near-surface layer of East Asia and Europe were investigated as well. To this end, we conducted model comparisons versus EANET and EMEP stationary observations for mass and gaseous

https://doi.org/10.5194/gmd-2021-385
Preprint. Discussion started: 3 December 2021


Geoscientific Model Development Discussions

concentrations of $PM_{2.5}$, SO_4^{2-}, NO_3^-, HNO_3, NO_x, O_3, and CO (CO for EMEP only). Table 5 shows the correlation coefficients (R) and model biases for each species in the OLD and STD cases. The OLD simulation has its fair correlations and RMSEs with observation for SO_4^{2-} (R(EANET) = 0.56, R(EMEP) = 0.63), NO_3^- (R(EANET) = 0.36, R(EMEP) = 0.713), and HNO_3 (R(EANET) = 0.181, R(EMEP) = 0.115), which are in line with other atmospheric chemistry models' R and RMSE values against EANET and EMEP (Brian et al., 2017), as also discussed in Ha et al. (2021).

Overall, the inclusion of HONO improved *the R* for $PM_{2.5}$, SO_4^{2-}, NO_3^-, O_3 (EMEP), and HNO_3 (EANET). The R estimates for HNO_3/NO_3^- are slightly improved because of the inclusion of HONO photochemistry (OLD→STD: 0.713→0.755 for NO_3^- in EMEP, 0.181→0.228 for HNO_3 in EANET, Table 4). However, its effects are not pivotal for modifying (increasing/decreasing) levels of NO_x, which is additionally underestimated in the STD run due to the NO_2 loss by heterogeneous processes (bias OLD→STD: -3.997→-4.358 for EANET). Figure 3 compares the measured versus simulated HNO_3, NO_x, HONO, O_3, and CO concentrations for the EANET and EMEP stations. The stations were divided into three groups: (1) high-NO_x EANET stations, including Jinyushan (China), Kanghwa, Imsil, Jeju (South Korea), Bangkok, Nai Muaeng, Samutprakarn, Si Phum (Thailand), Metro Manila (Philippines), and Ulaanbaatar (Mongolia); (2) other EANET stations (39 for HNO_3, 22 for O_3, and 15 for NO_x); and (3) all EMEP stations. The ground-based observations in the period 2010–2016 revealed the slightly decreasing NO_x for moderate NO_x concentrations, as well as $PM_{2.5}$, and aerosols (Figure 3(e,h) and Figure S4(e,g,h,i)). These decreasing trends were not captured by our simulations that used the high emission scenario for the EDGAR/HTAP-2008 inventory. Note that NO_x and $PM_{2.5}$ concentrations are generally underestimated in the model (OLD), especially in high-NO_x regions (Figure 3(b,e,h) and Figure S4(a,d,g)) with model's averaged biases of -0.8 ppb NO_x for EMEP and -4 ppb NO_x for EANET (Table 5). These underestimations were stronger during winter, particularly for the high-NO_x regions. It is possible that complex domestic sources could lead to diluted emissions for the simulations' moderate horizontal resolution (~2.8°). Higher model resolutions such as 1.1°, 0.56° or even higher, could remedy such effects (Sekiya et al., 2018). In the STD case, including HONO photochemistry, the negative biases of NO_x in the model have adversely increased due to the NO_2 loss processes. These processes also suppressed the observed NO_x seasonality observed at most sites (Figure 3(b,h), red lines). The lack of seasonality was driven by the substantial loss of NO_2 on the surfaces of atmospheric particles during winter. For EANET's low NO_x and EMEP stations, this huge NO_2 loss is attributed to cloud surfaces (Figure 3(ee,hh), blue bars). However, NO_2 uptake by aerosols has a comparable contribution effect to the cloud effect in high-NO_x environments such as Jinyunshan (Figure 3(bb), grey bars). Namely, nearly half of the NO_2 was converted to HNO_3 in R4 (Figure 3(aa,dd,gg)) without an efficient recycling process, leading to an overall removal of NO_x. This lack of NO_x could be the main driver for the seasonal NOx deterioration and for the exacerbated overestimations of HNO_3 by simulations.

The STD O_3 simulation exhibited moderate and strong positive correlations with EANET and EMEP observations, 0.595 and 0.707, respectively (Table 5). The improvements in the concentrations of SO_4^{2-}, NO_3^-, $PM_{2.5}$, and HNO_3 were minor, but that for O_3 was large with a bias reduction of ~67% for EMEP and ~74% for EANET (Table 4). In the STD case, too little NO_x is left from its heterogeneous loss, causing a net O_3 chemical destruction, which in turn, reduces the model overestimates for O_3 in the OLD case (Table 5; Figure 3(c,f,i), red versus blue lines). However, further improvements in the chemical scheme

https://doi.org/10.5194/gmd-2021-385
Preprint. Discussion started: 3 December 2021

Geoscientific Model Development Discussions

are necessary to reproduce the O_3 measurements better; namely, a larger O_3 reduction for the summer and a reduced effect in simulated O_3 for the winter might alleviate the undesired effects. A delayed minimum from summer (as observed) to early winter (calculated in OLD and STD runs) causing opposite seasonality for O_3 is prominent for the low-NO_x EANET stations (Figure 3(f)). Due to the O_3 reduction, the increment in CO for EMEP stations reconciles the model's underestimation of CO high peaks in spring (Figure 3(j)), thereby, strongly dwindling the bias for CO by ~59% (Table 4). However, the CO concentrations from May to the end of the year were overestimated in the STD run. This finding might indicate inadequate HONO emissions for the EMEP stations, which have a reducing effect and eliminate the model overestimates for CO (Figure 3(jj): oranges). In general, the verifications with EANET and EMEP showed that HONO impacts on NO_x, O_3, and CO were vastly dominated by cloud uptakes, except aerosol effects on NO_x for high-NO_x regions.

To solve the problem of underestimated NO_x abundances and the ill-reproduced seasonality mentioned above, an explicit inventory for surface NO_x emissions and/or a NO_x recycling process is required. Figure 3(aa,dd,gg) shows that the improvements in the HNO_3 simulation could arise due to higher NO_x emissions and strengthening aerosol uptake. Such a recycling mechanism via the reaction $HNO_3 \rightarrow NO_2$ (R7) on soot particles (Lary et al., 1997; Akimoto et al., 2019) was also investigated by changing the HNO_3 uptake coefficient for HNO_3 from 3×10^{-5} to 4.6×10^{-3}. Unfortunately, implementing R7 in CHASER could not successfully recycle NO_x for the EANET and EMEP sites (the result is omitted). Furthermore, intensifying heterogeneous HONO formation in summer might further reduce O_3, as discussed in Section 3.1.5.

Table 5: Model comparison of different species with observations at the EMEP and EANET stations. Three-sigma-rule outlier detection is applied for each station before calculating correlation coefficients *R*. NO_x data are filtered once more using the two-sigma-rule. *R* and bias of the STD run are shown as bold if improved compared to the OLD run. Units for model biases for $PM_{2.5}$, SO_4^{2-}, NO_3^-: μm m^{-3}; HNO_3, NO_x, O_3, CO: ppb.

	EMEP							EANET					
	$PM_{2.5}$	SO_4^{2-}	NO_3^-	HNO_3	NO_x	O_3	CO	$PM_{2.5}$	SO_4^{2-}	NO_3^-	HNO_3	NO_x	O_3
R(STD)	**0.528**	**0.655**	**0.755**	0.115	0.637	**0.707**	0.526	0.344	**0.560**	0.359	**0.228**	0.202	0.595
R(OLD)	0.469	0.631	0.713	0.115	0.698	0.650	0.535	0.357	0.559	0.364	0.181	0.235	0.613
bias (STD)	**-2.494**	0.889	0.632	**0.073**	-1.680	**-1.708**	**2.943**	**-7.231**	1.161	**-0.223**	0.396	-4.358	**1.410**
bias (OLD)	-3.044	0.752	0.247	0.077	-0.818	5.154	-7.138	-7.583	0.981	-0.439	0.302	-3.997	5.494

https://doi.org/10.5194/gmd-2021-385
Preprint. Discussion started: 3 December 2021

Geoscientific Model Development Discussions
Open Access
EGU

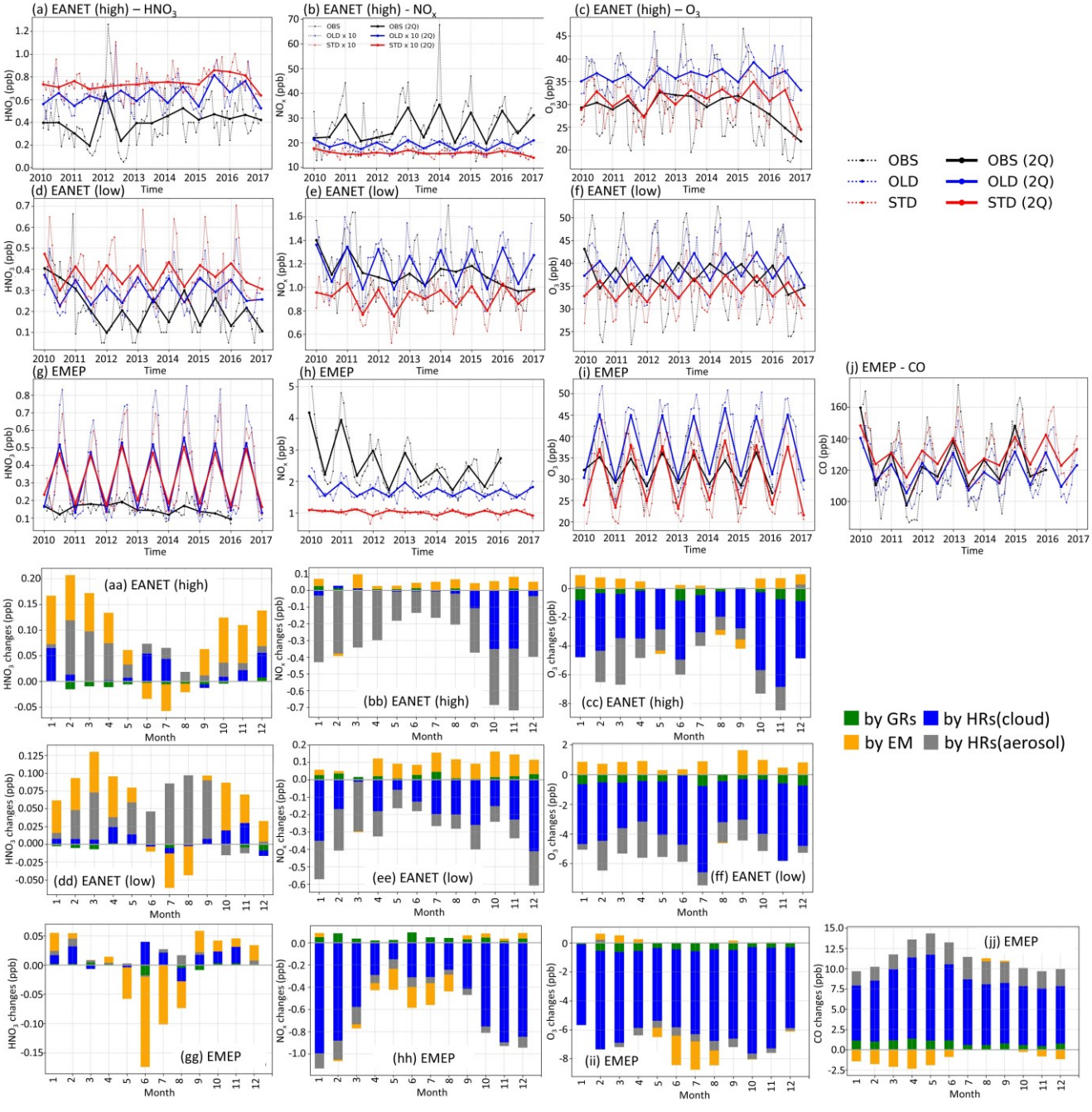

Figure 3: Concentrations and changes by HONO inclusion for EANET and EMEP stations. (a-j) Observed and simulated concentrations during 2010–2016. Black lines: observation; red: STD case; blue: OLD case. In (b), concentrations in STD and OLD are 10 times-folded for better visualization (red and blue lines). For each group of stations, dotted lines are all stations' median from each station's monthly-mean values. Thick solid lines represent two quarters averaged from dotted lines. (aa-jj) Calculated monthly-mean changes by HONO chemistry. Green bars: monthly changes by GRs; blue: by HRs on clouds; grey: by HRs on aerosols; orange: by EM. Stations are grouped as high-NO_x EANET (first and fourth rows), low-NO_x EANET (second and fifth rows), and all EMEP stations (third and sixth rows). First column: HNO_3; second column: NO_x, third column: O_3, fourth column: CO.

https://doi.org/10.5194/gmd-2021-385
Preprint. Discussion started: 3 December 2021


Geoscientific Model Development Discussions
Open Access
EGU

3.1.3 Effects of HONO chemistry in coastal regions

The simulations also compared with the *research vessel (R/V) Mirai*'s observation in the western Pacific Ocean for O_3 and CO. The interpolation of model results for six cruises across Japan–Alaska region (40° N– 75° N, 140° E–150° W) in 7-8-9/2015–2017 (summer), Indonesia–Australia region (5°–25° S, 105–115° E), and Indonesia–Japan region (10–35° N, 129°–140° E) are provided for the period of 12/2015 - 1/2016. All the measured and simulated data were provided, whereas the data for the NP region (40°–60° N) were analyzed separately, as discussed in Section 3.2. More detailed information about the *R/V Mirai* can be found in Kanaya et al. (2019). Furthermore, the model evaluation with *Mirai* for the OLD run can be found in Ha et al. (2021).

Table 6 shows correlation coefficients, which indicate that the STD simulation for CO and O_3 agree well with *Mirai* (R =~0.6). However, these correlation coefficients are slightly worsened, compared with the OLD case. Although the HONO inclusion mostly reduces the model bias for CO, especially in the NP region (-16.158 to -4.948 ppb), the model bias for O_3 is increased. The model biases exhibit negative trend for both CO and O_3 in the OLD case. This simulation pattern for O_3 in the NP region is in line with the OMI comparison (Sect. 3.1.1). This finding seemingly indicates an insufficient downward mixing process of O_3 in the free-troposphere or inconsistent surface deposition (Ha et al., 2021; Kanaya et al., 2019). However, the CO underestimations in the NP region might mark the inadequate CO emission in the HTAP inventory in CHASER (Ha et al., 2021). In Figure 4(a,c), overestimations of CO and O_3 are visible along Japan-Indonesia-Australia (Track-2) during the low episodes in December/January. Here, the larger model biases might account for the model's insufficient halogen chemistry (Kanaya et al., 2019; Ha et al., 2021). Figure 4 shows the model's percentage discrepancies for O_3 from *Mirai*'s data, except those from HONO concentrations interpolated for these regions. The underestimated simulations of O_3 are enlarged, especially in the Japan – Alaska region, being driven by the reduction effects in the STD case. In other way, these effects weaken the O_3 overestimates across the land areas, namely, over the region near Japan and near Indonesia-Australia. Moreover, the higher HONO levels are identified for these off-shore data with up to 1.4 ppb abundances (Figure 4(c): red numbers). This high HONO level might be and underestimation of a true level as a stronger reduction for O_3 is required for the STD run (Figure 4(a): red marks).

The effects of the HONO chemistry along *the R/V Mirai* tracks exhibit various trends for each mechanism. Figure 5(b,d) illustrates O_3 and CO changes, triggered by the HONO gas reactions (GRs), uptakes (HRs), and emission (EM). The gaseous reactions (blue bars) have mostly increased CO level, except some reductions at the peak CO level for the NP region. Furthermore, O_3 level is slightly increased due to GRs north of 60° N, but is also often decreased in the NP region and varies near land areas. HRs, largely consuming NO_2, reduced O_3 (as large as 8 ppb), and increased CO (~10 ppb) levels (Figure 5(b,d): orange+green). HRs, (particularly HRs on cloud surfaces, shown by orange bars), exerted the strongest contribution to the calculated changes in O_3 and CO among the three HONO pathways. This predominant cloud effect was also prominent in the previous comparisons, especially EMEP (Figure 3(ii,jj): blue), thereby, indicating substantial effects of clouds at the mid-latitudes where the cloud SAD is higher (Figure S1). HRs on aerosols (green bars) have minor contributions during all cruises,

https://doi.org/10.5194/gmd-2021-385
Preprint. Discussion started: 3 December 2021

Geoscientific Model Development Discussions

despite they caused a marked increase in the O_3 concentrations off-coast Japan (track #3). It should be noted that this is not enough to explain the simulation bias with regards to the measurements. The additional HONO from direct emission (red bars) has mainly increased O_3 and has reduced CO concentrations, especially near land (latitude < 50° N). This finding resonates with the comparison for continental stations (Figure 3(cc,ff,ii,jj): oranges). The overall effects of the HONO chemistry along *Mirai* cruises tend to reduce O_3 and to increase CO levels. For the NP region, CO level increase and OH revel reduction also can ameliorate the model performance. The improved model performance is evidenced from the comparison of the simulation with aircraft data as well (Figure 7(g,h)). Thus, the strengthened underestimation of O_3 concentration in the NP region is unlikely driven by HR on cloud particles (Sect 3.1.1 and Ha et al., 2021). It is rather related to the inconsistencies in the surface deposition of ozone. These inconsistencies are supported by empirical evidence as the negative bias in this comparison turns neutral or positive for the aircraft measurements in the same region (Figure 7(f): at 1000 hPa). The latter pattern is shown in the next section of this study as well.

Table 6: Model comparison with *Mirai* cruises: no outlier filter is applied. *N* is the available data for each calculation. Correlation coefficient (*R*, no unit) and biases (ppbv) in STD run are shown as bold if better than those in OLD run.

	CO ***N*=4030**	**CO (40–60° N)** ***N*=1374**	**O_3** ***N*=3893**	**O_3 (40–60° N)** ***N*=1418**
R(STD)	0.690	0.586	0.568	0.618
R(OLD)	0.696	0.601	0.628	0.642
bias (STD)	**4.087**	**-4.948**	-8.823	-7.823
bias (OLD)	-8.136	-16.158	-3.625	-1.472

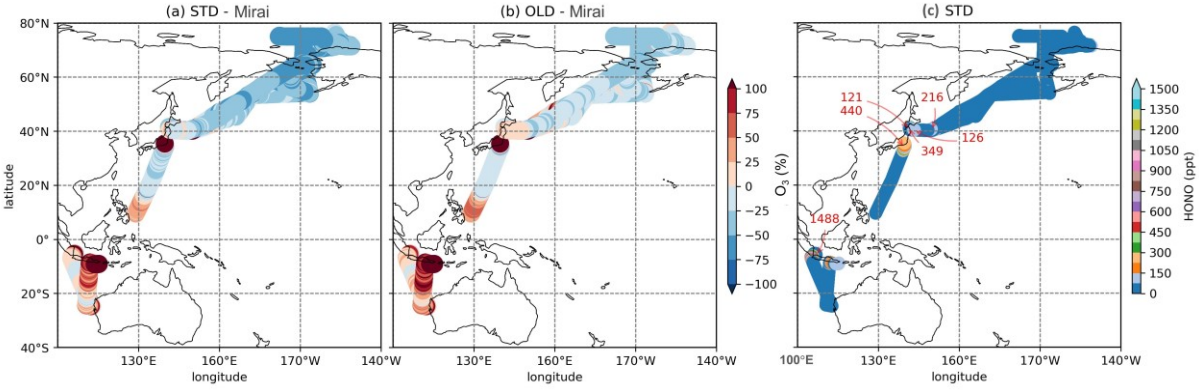

Figure 4: Percentage discrepancies of STD (a) and OLD (b) simulations from *Mirai* for O_3 and HONO concentration in STD (c). The red numbers in (c) indicate maximum HONO concentrations for each cruise.

https://doi.org/10.5194/gmd-2021-385
Preprint. Discussion started: 3 December 2021

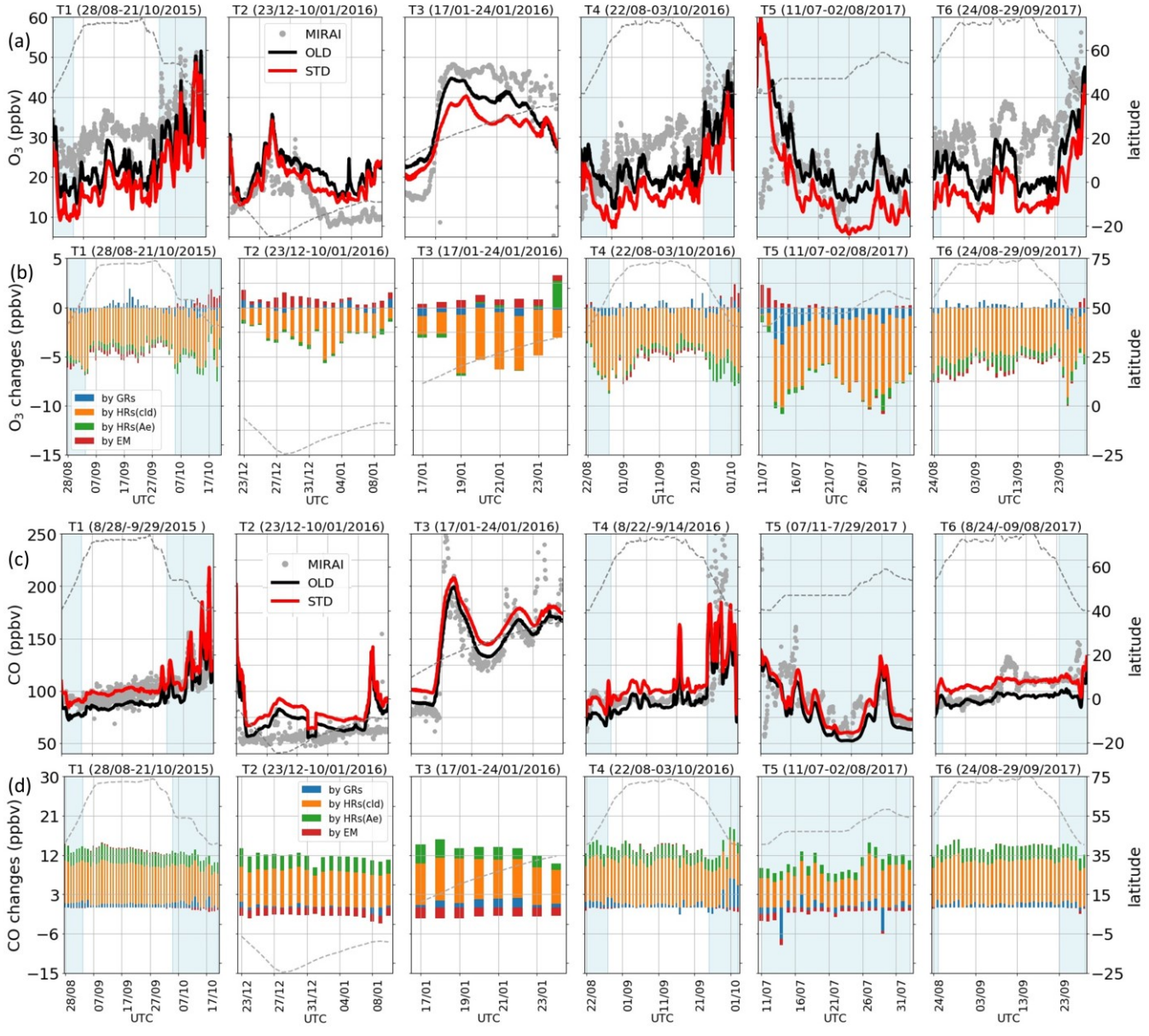

Figure 5: Validation with ship-based data. Observed and simulated concentrations (a, c) and daily mean effects by HONO chemistry (b, d) for O_3 and CO during *Mirai* cruises. In (a, c), grey dots: observation, black lines: OLD case, red lines: STD case. In (b, d), blue bars: changes by GRs; orange: by HRs on clouds; green: by HRs on aerosols; red: by EM. The left axis exhibits the concentrations and changes (ppbv). The right axis shows cruising latitudes plotted as dashed lines. The horizontal axis is travel times (UTC). Vertical light-blue shaded areas are for data in the NP region (140–240° E, 40–60° N).

https://doi.org/10.5194/gmd-2021-385
Preprint. Discussion started: 3 December 2021


Geoscientific Model Development Discussions

3.1.4 Effects of HONO chemistry in the free troposphere

The model performance of the free troposphere was evaluated through the atmospheric tomography (ATom1) aviation in August 2016 for NO_2, OH, CO, and O_3. The STD run reconstructed the chemical field observed in ATom1 with moderate or strong positive correlations for NO_2, OH, CO, and O_3 (R_{NO2}=0.730, R_{O3}=0.751, R_{OH}=0.579, R_{CO}=0.659; Table S2). For the NP region, the model correlations for these species were slightly lower (R_{NO2}=0.621, R_{O3}=0.609, R_{OH}=0.407, R_{CO}=0.596; Table S2). The *R* values for NO_2 and CO were always higher in the STD run, compared with those in the OLD run, while for OH and O_3, the *R* values are only improved for the NP region (Table S2).

Figure 6 shows measured (grey) and simulated (red and black) NO_2, O_3, OH, CO concentrations and the effects of including HONO in the simulation for the NP region (flight #2 on August 3rd). Figure 7 displays vertical profiles of the HONO chemistry's model biases and photochemical effects. Here, the data in all flights or in NP region are classified based on the air pressure from 1000–200 hPa (±50 hPa) and separated on nine bins. In the NP region, the OLD run (black lines) tends to overestimate NO_2, O_3, OH, but it underestimates CO at the lower troposphere, whereas the unsteady discrepancies at the upper layer are visible (Figure 6(a,b,e,f)). All four species tended to be underestimated near the tropopause (300–400 hPa) and to be overestimated in the lower stratosphere (Figure 7(e-h). The HONO inclusion in STD run (red lines) has reduced NO_2, OH, O_3 and has increased CO levels, thereby, dwindling the model biases for NO_2, OH, and CO in the NP region except near the tropopause (Figure 7(e,g,h)).

In the NP region, the surface NO_2 level is reduced under the effects of HONO uptake on clouds (Figure 6(c): orange bars in vertical pink shades and Figure 7(p)). Hence, O_3 and OH are correspondingly reduced as their formations are limited in the absence of sufficient NO_x, that is, OH formation via $HO_2 + NO \rightarrow OH + NO_2$ (Figure 6(d,g): orange bars in pink columns and Figure 7(q,r)). Near the surface, aerosol HRs only slightly affected atmospheric species, whereas at high altitudes, the aerosol uptake is more relevant to the OH, O_3, and CO concentrations (Figure 6(c,d,g,h) and Figure 7(q-s): green bars). The dominant cloud effects near the surface appear plausible for an ocean region with high cloud fractions at the lowest layer (Figure S2). GRs also affect OH, O_3, and CO, whereas the effects are rather manifested in the upper troposphere than in the lower troposphere. This is likely the most influential factor that increases OH and O_3 levels at these high altitudes (Figure 6(d,g) and Figure 7: blue bars). The additional HONO from direct emissions had minor effects on NO_2 and OH but contributed to the reductions of O_3 and CO at high altitudes (Figure 6(c,d,g) and Figure 7(q,s): red bars). At 900 hPa, the HONO emissions significantly reduced NO_2 near the continental areas (Figure 7(l): red bars) due to its uptake by particles. These effects of the HONO chemistry in the STD simulation somewhat reduce the model biases for NO_2, O_3, OH, and CO (Figure 7(a-h): red numerical texts are the percentage reduction in model bias). Note that these biases are very pronounced near-surface (~1000 hPa) in the NP region (51.7% for NO_2, and 77.3% for OH). To capture the patterns identified by observations in the upper troposphere, except the NP region, more robust increases for NO_2 and OH levels are still required (Figure 7(a,c)). At these altitudes, NO_x and HO_x sources from lightning (Brune et al., 2021) or aviation can be relevant, as discussed in Section 3.1.5.

https://doi.org/10.5194/gmd-2021-385
Preprint. Discussion started: 3 December 2021


Geoscientific Model Development Discussions
Open Access
EGU

Overall, the comparisons between the model and *Mirai* and ATom1 may indicate that the HRs on cloud surfaces are the main contributing factor to the marine boundary's photochemistry, whose effects emerged during the ATom1 flights in the marine atmosphere. GRs and aerosol HRs exert stronger impact on atmospheric chemistry at higher altitudes, compared with the near-surface layer. Also, their effects should be enhanced through the supplemental NO_x and HONO sources to reconcile the model simulations with the observations.

https://doi.org/10.5194/gmd-2021-385
Preprint. Discussion started: 3 December 2021

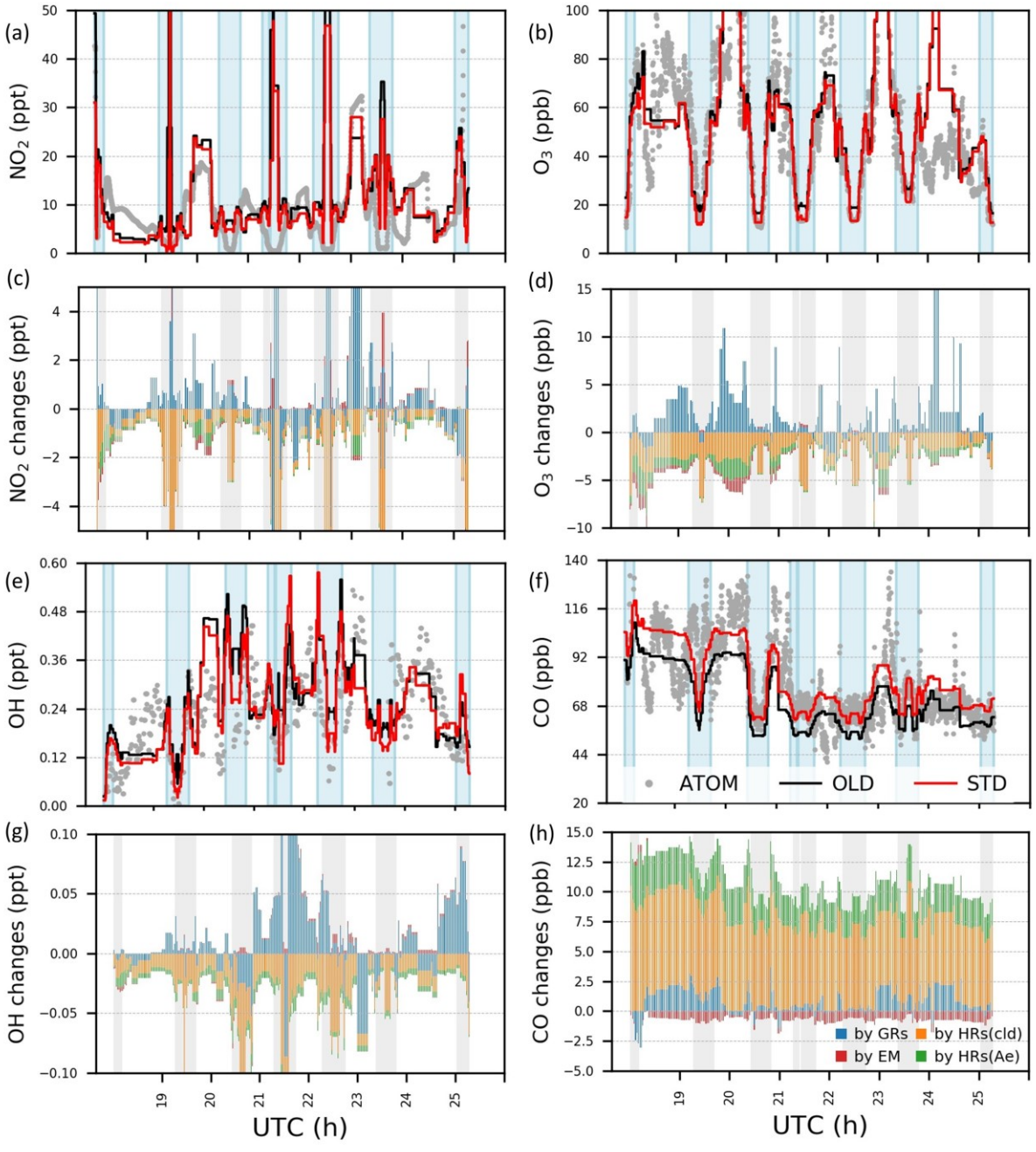

Figure 6: Concentrations and variations by HONO chemistry for NO_2, O_3, OH and CO during ATom1 flight #2 (198–210° E, 20–62° N). In (a-b, e-f), concentrations by observation (grey dots), simulations in OLD case (black lines), and in STD case (red lines) are plotted. In (c-d, g-h), changes in concentrations by GRs (blue bars), EM (red), HRs on clouds (orange), and HRs on aerosols (green) are plotted. Vertical blue and grey columns reflect the data for the regions with air pressure $P > 500$ hPa.

https://doi.org/10.5194/gmd-2021-385
Preprint. Discussion started: 3 December 2021

Geoscientific Model Development Discussions

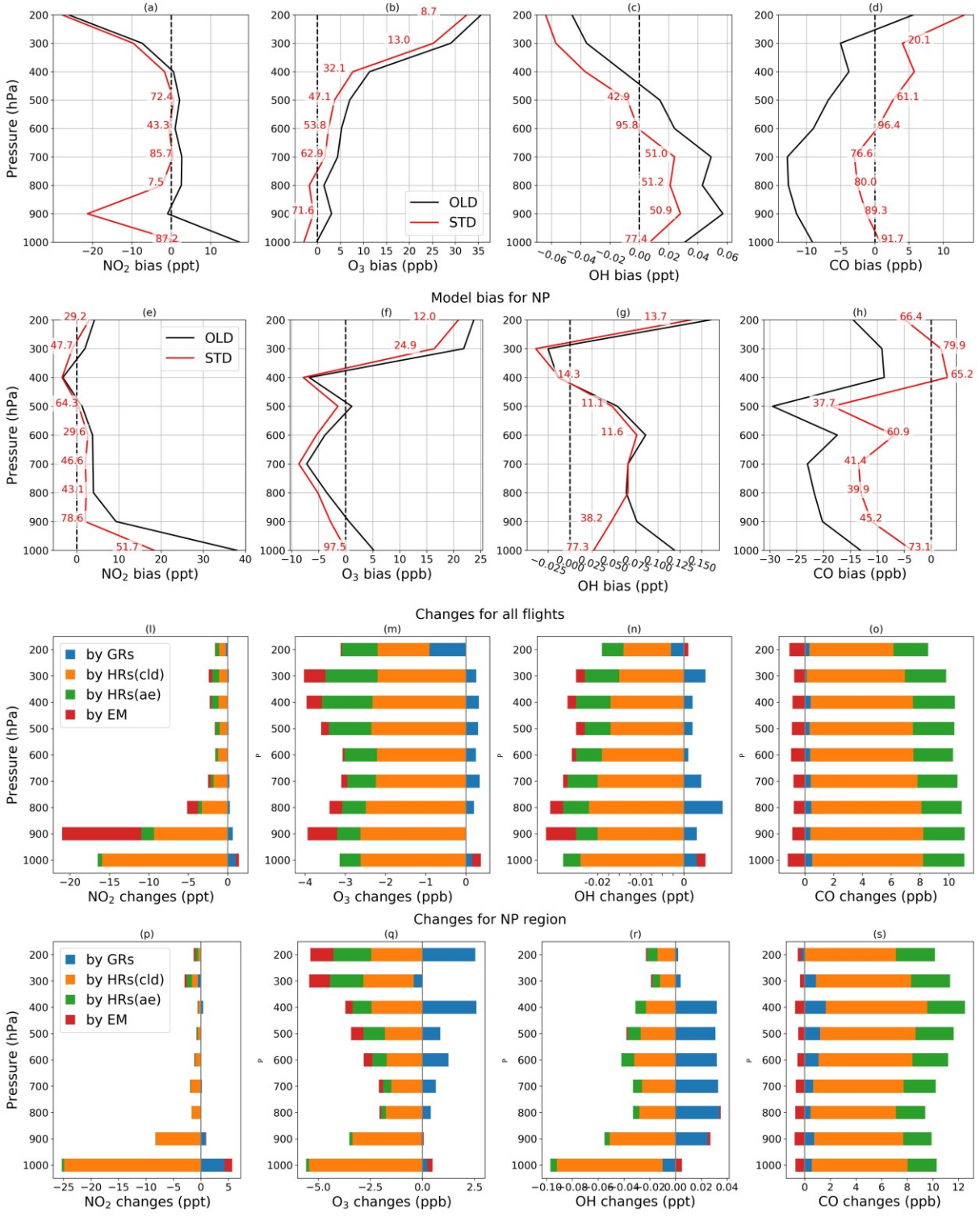

https://doi.org/10.5194/gmd-2021-385
Preprint. Discussion started: 3 December 2021


Geoscientific Model Development Discussions

Figure 7: Vertical profile of model bias against aerial ATom1 data (a-h) and changes by HONO chemistry (l-s) for NO_2, O_3, OH, and CO (from left to right columns). Biases in OLD (black lines) and STD (red lines) runs are calculated for all flights (a-d) and NP region (e-h). The red numerical texts are the relative reductions (%) of the bias in the STD run compared to that in the OLD run. Changes by GRs (blue), HRs on clouds (orange), HRs on aerosols (green), and EM (red) are calculated for all flights (i-o) and NP region (p-s).

3.1.5 Comparison of measured and simulated HONO concentrations at daytime

In this section, CHASER-based HONO estimates were evaluated by using the HONO measurements, collected during the EMeRGe campaign off-coast eastern Asia in spring 2018 (Andrés Hernández et al., 2021). The HONO measurements in the free troposphere could provide essential information on the underlying gas-phase and heterogeneous HONO formation mechanisms as most current HONO measurements were conducted in the surface air. The daytime HONO concentration was retrieved from the aircraft-borne limb measurements using the HALO mini-DOAS (differential optical absorption spectroscopy) instrument, in which the UV light (310–440 nm) absorbed by HONO was detected (Hüneke et al., 2017). The mini-DOAS's measurement method relies on near-UV/VIS/IR skylight spectroscopy in nadir and limb geometry. Data evaluation consists of three steps: (1) retrieval of slant column densities (SCDs) of trace gases by the DOAS method (Platt and Stutz, 2008), (2) forward radiative transfer modeling for each measurement using McArtim (Deutschmann et al., 2011); and (3) retrieval of concentration through a new scaling method for UV/VIS data (Stutz et al., 2017; Hüneke et al., 2017; Werner et al., 2017; Kluge et al., 2020; Rotermund et al., 2021).

Additional sensitivity runs were conducted to explore potential HONO sources during the daytime (Table 7). The correlation coefficient (R) and model biases against EMeRGe for HONO are shown in Table S3. As seen, general underestimations of HONO simulations are identified, in which better correlations are found at 1000–2000 m by the STD run (0.31–0.49). Vertical profiles for HONO and other species (NO_2, O_3, CO), retrieved from the EMeRGe flights were applied for the measurement-based model evaluation (Figure 8). The model discrepancies for the measurement for HONO (Δ_{HONO}) and NO_2 (Δ_{NO2}) in each flight trajectory, i.e., from Taiwan to South Korea, Japan, and the Philippines, are separated into bins of altitude ranges 0, 1000, 3000, 5000, and 6000 m (Figure 9). The frequency distributions of Δ_{HONO}, Δ_{NO2}, Δ_{O3}, and Δ_{CO} are shown in Figures S7 and S8. Plots similar to Figure 9 but for all cruising altitudes (0–8000 m) are shown in Figure S9, and those for O_3 and CO are shown in Figures S10 and S11, respectively.

Figure 8(a) shows the vertical average score (cruising altitudes ± 500 m) for the measured (blacks) and simulated HONO concentrations in STD (reds) and those results of sensitivity cases. The measured daytime HONO concentration was close to the boundary layer (below 1,000 m) over Taiwan, averaged at 115 ppt, and was peaked at ~250 ppt. Also, the HONO concentration decreased up to 9,000 m, with mean values dropping from 70 ppt (2000 m) to < 20 ppt (5000 m) and < 10 ppt above. Unexpectedly, the simulated HONO concentration (STD) significantly underestimated the observations. They reached only 30–70 ppt at 1,000 m and nearly zero from 2,000 m upward (Figure 8(a): red versus black triangles for the simulation and the observations, respectively). These discrepancies indicate a significant unknown HONO source during the daytime, despite the proposed heterogeneous HONO formation mechanisms were incorporated in our model. This finding adds another

https://doi.org/10.5194/gmd-2021-385
Preprint. Discussion started: 3 December 2021


Geoscientific Model Development Discussions

instance of evidence about missing HONO sources in the polluted boundary layer and free troposphere (e.g., Kleffmann et al., 2003; Li et al., 2014; VandenBoer et al., 2013; Xue et al., 2021a; Ye et al., 2018).

A previous study addressed the altitudes below 300 m, where HONO deposited onto the ground surface at night, and further proposed to be a significant reservoir for HONO during the day (VandenBoer et al., 2013). However, this source may only affect the lower boundary layer, while only insignificantly contributing to the tropospheric HONO budget (Ye et al., 2018; Zhang et al., 2009). Such a parameter for ground surfaces in a global model is somewhat uncertain, whereas the missing daytime HONO is still identified at 5000 m altitude. Thus, the amplified existing mechanisms and the additional sources for HONO in the free troposphere are examined in this study as well.

As the implemented HR HONO formation processes was likely insufficient, a series of additional sensitivity simulations was performed as well (Table 7). The AIRC case is aimed to evaluate another source of HONO emission, that is, aircraft emissions of HONO with a HONO/NO_x emission by a factor of 0.4. In the EMx8 case, the HONO/NO_x emission factor is amplified up to 0.8 (=0.1 in STD case), being focused to emphasize the sensitivity of HONO's direct source from the ground layer, especially from soils as suggested by the previous study (Oswald et al., 2013). In the GRx8 case, the rate constant of (R2) is eightfold with the increase in homogeneous HONO production, given the fact that the daytime missing HONO could be relevant to other gas-phase formations (Romer et al., 2018; Li et al., 2014). Furthermore, the factor 8 applied in EMx8 and GRx8 cases were selected after testing with factors 2 and 4, aiming for simulations to agree with the measurements. In the maxST case, the uptake coefficients (γ-values) of NO_2 on organic and black carbons are maximized to 0.1 (R4, R5). Results from the maxST case can be used for estimation of the separate role of soot uptake under daytime conditions (George et al., 2005; Monge et al., 2010; Ndour et al., 2008), which could achieve an unrealistically high γ-value of 10^{-1} to 10^{-8} (Ammann et al., 1998; Kalberer et al. 1999). The ratR4 case is run in an attempt to produce more HONO from heterogeneous sources by altering the HONO: HNO_3 yield ratio in (R4) to 0.9: 0.1. The last case, ratR4+CLD, is the same as the ratR4 case, except for $\gamma_{liq.}$ increased a hundred-fold ($1e^{-4}$ → $1e^{-2}$). The main idea here is to evaluate whether the missing HONO source was sensitive to cloud uptake in this region or not.

Table 7: Additional sensitivity simulations in this work.

No.	Simulation ID	Description	Note
1	AIRC	aircraft HONO emission = 0.4% aircraft NO_x emission	Not applied in STD
2	GRx8	Rate (R2) × 8	
3	EMx8	EM(HONO) = 0.8 NO_x emission	= 0.1 in STD
4	maxST	γ_{oc} and γ_{ec}(R4, R5) = 0.1	See Table 2 for γ-values in STD
5	ratR4	NO_2 → 0.9HONO + 0.1HNO_3 (R4)	Product ratio is 0.5:0.5 in STD
6	ratR4+CLD	ratR4 and $\gamma_{liq.}$(R4) = 0.01	= 0.0001 in STD

In the model, the measured NO_2 below 3000 m (±500 m) close to land was captured well (Figure 9(a,d,h): magentas and greens), with 34% of the data being quite close for NO_2 (±70 ppt) (Figure S7(d)). However, the simulated HONO mixing ratio

https://doi.org/10.5194/gmd-2021-385
Preprint. Discussion started: 3 December 2021


Geoscientific Model Development Discussions

is still underestimated by the modeling by up to 250 ppt (Figure 9(a): green). Over the off-coast of Taiwan bound to Japan, NO_2 was overestimated by up to 600 ppt in the model, corresponding to 20–70 ppt missing HONO (Figure 9(a,d): small oranges left of vertical line). The missing HONO can be driven by the low uptake of NO_2 on organic carbon and soot, as the amplified maxST cases could alleviate the model underestimates for HONO (Figure 9(a,d) versus (c,f)). The maxST run further reduces NO_2 level, thereby, implementing these cases in practice requires a more efficient recycling of NO_x. Besides the uptake on organic and black carbon, identified in the maxST simulations (they are the most efficient HONO producers), we identified the NO_2 uptake on sulfate nearly as important through a parallel test (not shown). For the middle troposphere (5000–6000 ± 500 m) over the Taiwan Island, too abundant NO_2 is predicted by the model during the cruises bounding to South Korea (up to 40 ppt) and the Philippines (up to 20 ppt) (Figure 9(k,n): small greens and blues left of the vertical line). These overabundances might hint on the deep stratospheric intrusion in springtime that caused imperfect downward mixing fluxes (Lin et al., 2012; Stohl et al., 2003; Trickl et al., 2014). This excessive NO_2 and the corresponding missing HONO are also sensitive to the AIRC and GRx8 cases (Figure 9(k,n) versus (l,m)), indicating that aircraft-exhaust of HONO could adjust the HONO/NO_2 ratio and more homogeneous HONO production might contribute more, given the high abundances of oxidizing substances at these altitudes.

The model underestimation for HONO is also associated with the concurrent underestimation of NO_2, which was observed more often at the altitudes of > 1000 m. The likely erroneous NO_2 concentrations of ~1.8 ppb (1000 m) and ~220 ppt (3000 m) across Taiwan, linked with HONO of as high as 290 ppt (1000 m) and 140 ppt (3000 m), were not reproduced (Figure 9(d,h)). These likely inadequate NO_2 abundances can be partially alleviated through the enhanced HONO/NO_x emission ratio and more efficient NO_x recycling process in the EMx8 and ratR4+CLD cases, respectively (Figure 9(e,g,i,j)). Here, the missing HONO is largely supplemented only at ~1000 m over the marine environment, namely, during the Taiwan-Japan cruise, when we identified more product for HONO on cloud in the ratR4+CLD case. (Figure 9(d,g): red-orange diamonds). At ~6000–8000 m, small deficits of 60 ppt NO_2 corresponding to ~10 ppt HONO (Figure 9(e-i): small oranges and magentas) might correspond to lightning NO_x emissions (Sudo et al., 2002) and stratospheric sources. There were no heterogeneous or emission cases that succeeded in providing more HONO at this height, but some homogeneous mechanisms at ~6000 m as in the GRx8 case could be effective (Figure 9(n,o)).

However, these sensitivity cases only correspond to at most 35–45 ppt elevated HONO at ~1000 m (by maxST) for a total of 110–115 ppt HONO underpredicted (Figure 8(a)), requiring more efficient HONO formation mechanism. The model also underestimated O_3 and CO by less than 25 ppb (freq. 79%) and 100 ppb (freq. 60%), respectively (Figures S10, S11), which are larger than the model biases against ATom1 observations (Figure 7) because of possible inland influence. A further scrutiny of the higher proportion of HONO emissions and the increased uptake efficiencies for aerosols at 0–500 m and clouds at 1000 ± 500 m are recommended. For the boundary layer, the daytime HONO concentrations could be enhanced with a more accurate and detailed emission inventory for substances such as NO_x and CO. This is sensible as this region is the outflow of the Pearl River Delta and Yangtze River Delta regions. To capture the measured patterns at the middle-to-high altitudes, NO_2 and O_3 levels should be adjusted through more sophisticated vertical mixing and downward fluxes of NO_x and O_3 from the

https://doi.org/10.5194/gmd-2021-385
Preprint. Discussion started: 3 December 2021


Geoscientific Model Development Discussions

stratosphere. The possibility of aircraft engine emissions should also be investigated further by elucidating the role emissions of aviation-induced particles on which NO_x to HONO conversion could reach 45% (Meilinger et al., 2005).

The upper limit for the aerosol uptake coefficients (maxST case) may be applicable for the lowest cruising altitudes, which induced the increase of modeled HONO levels during both daytime and nighttime. For instance, the averaged summer mean of HONO in surface air reached the maximum at 0.8 ppb in the STD simulation, and it substantially increased up to 1.8 ppb in maxST (Figure S13(b): greens), thereby, alleviating the bias with regards to measurements (i.e., 2.0 ppb), reported in other studies (Li et al., 2012). This increase in the nighttime HONO level is also visible in the ratR4 simulation, but is twofold weaker, compared to that in maxST (Figure S12: blue). Moreover, the strong aerosol uptake parameters further reduced O_3 concentrations down to the measured minima in summer (Figure S12(d,e,f): blues versus greys, as discussed for the continental data (Section 3.1.2)). The simulations with R4's product-ratio HONO/HNO_3 as large 9/1, enhancement for both NO_2 and O_3 compared to the STD case are expected given less NO_x loss via HNO_3 deposition. However, the enhanced uptake of clouds, applied in ratR4+CLD would reduce O_3 concentration below 2500 m instead (Figure 8(b,d): browns < reds) as HNO_3 can affect the O_3 concentrations via renoxification mechanisms (Schneider et al., 1998). In fact, the HONO chemistry affects minor NO_x concentrations, compared to the product ratio 1:1 ratio in (R4) with the trial product ratio. In this way, the original NO_x seasonality (Figure S12: cyan) is retained and the problem with NO_x seasonality is mitigated (see details in Section 3.1.3). The trial ratio in R4 produced more HONO without disturbing the seasonal variability of NOx, thus leading to more OH. This effect on the OH concentration (ratR4) results in a slight increase in the CH_4 lifetime, but less than in the STD case (+5.6% versus +13.1%). If (R4)'s product ratio towards more HONO formation is plausible, the impact of HONO on the tropospheric oxidizing power should be much smaller than that discussed in Section 3.2.2.

The photolysis of particle-phase NO_3^- (aNO_3^-) < 300 nm has been previously suggested as a supplemental NO_x source (Romer et al., 2018) which might be another remedy for the inaccurate NO_x seasonality in this study. Moreover, aNO_3^- photolysis can be the efficient HONO production mechanism during the daytime in an aqueous environment with low pH and the presence of OH scavengers (Benedict et al., 2017a; Benedict et al., 2017b; Ye et al., 2018). This mechanism is valid, despite the produced HONO may be destroyed by the liquid-phase OH (Scharko et al., 2014). To apply this particle-phase photolysis to a model as an efficient HONO source, one needs to apply sophisticated computation of VOC and OH. Moreover, another light-dependent gas-phase HONO source might lead to a cycle with zero net production of HONO, NO_x, and HO_x, that is, $HO_2.H_2O + NO_2 \rightarrow$ HONO followed by HONO photolysis (R1) (Li et al., 2014). In CHASER, only gas-phase NO_3^- photolysis was introduced with the only channel to regenerate NO_2. The suggested reaction $HO_2 + NO_2 \rightarrow HONO + O_2$ (Burkholder et al., 2015) was introduced, but it did not successfully preserve the total reactive nitrogen chemistry (NO_y); hence, it was omitted in this study. The remaining drawbacks in reproducing HONO and other atmospheric species (NO_2, O_3, CO) by model urges further elucidation of more efficient HONO formation mechanisms. To this end, one needs (1) to provide better emission inventories for anthropogenic sources of pollutants from Southeast Asia and East Asia, lightning-produced NO_x and HO_x, and aviation-induced aerosols, (2) to improve the vertical mixing and air mass transport from the stratosphere, (3) to apply other potential HONO formation mechanisms and NO_x recycling processes alongside the selection and algorithm development

https://doi.org/10.5194/gmd-2021-385
Preprint. Discussion started: 3 December 2021

Geoscientific Model Development Discussions

among the sensitivity tests provided here; and (4) to simulate the lower and upper limits for the uptake coefficients of NO_2 on aerosols and clouds.

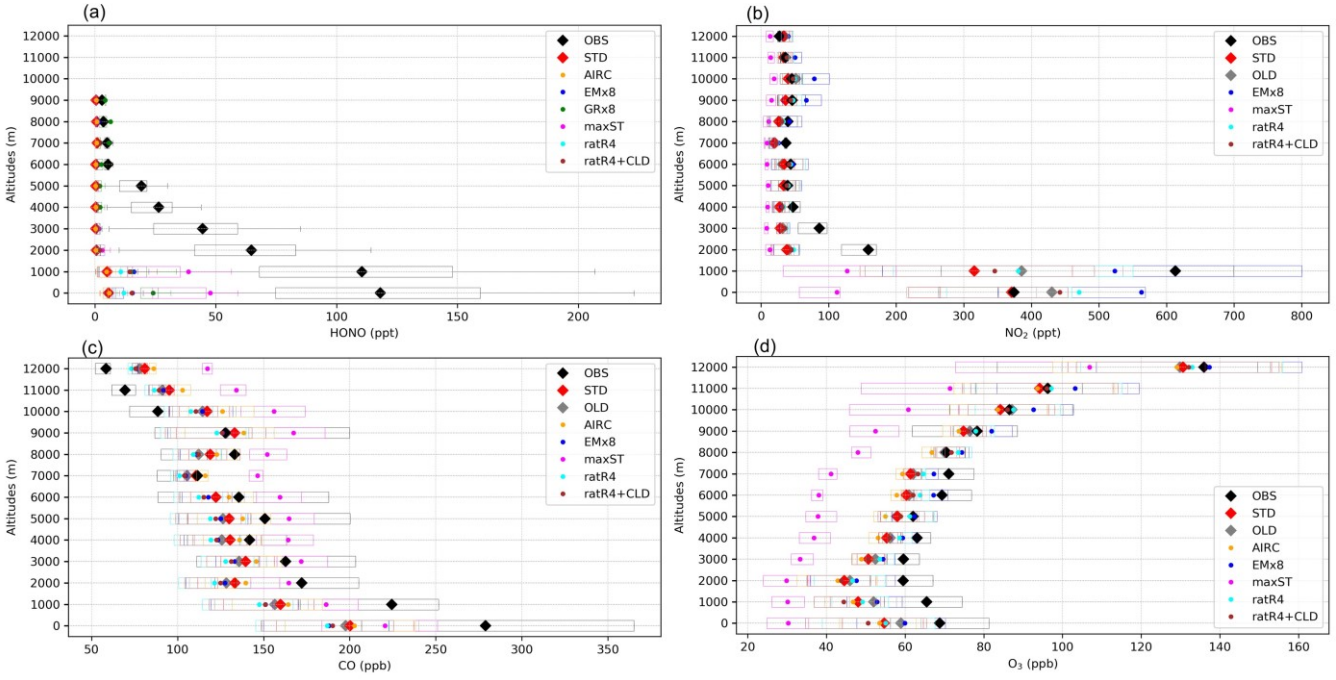

Figure 8: Vertical profiles of (a) HONO, (b) NO_2, (c) CO, and (d) O_3 measured in EMeRGe campaign and calculated in sensitivity runs. Diamonds (for OBS, STD, OLD) and dots (for other runs), boxes indicate mean, 25th and 75th values, respectively. In panel (a), whiskers with two caps show min and max HONO levels; all sensitivity runs are shown except OLD (the case without HONO chemistry). In (b), AIRC and GRx8 runs are omitted due to minor effects and obscured by STD run. In (c), (d), GRx8 run are omitted for the same reason and obscured by AIRC run. Colours are black for observation, red for STD run, orange for AIRC run, green for GRx8, blue for EMx8, magenta for maxST, cyan for ratR4, and brown for ratR4+CLD, grey for OLD.

https://doi.org/10.5194/gmd-2021-385
Preprint. Discussion started: 3 December 2021

Geoscientific Model Development Discussions

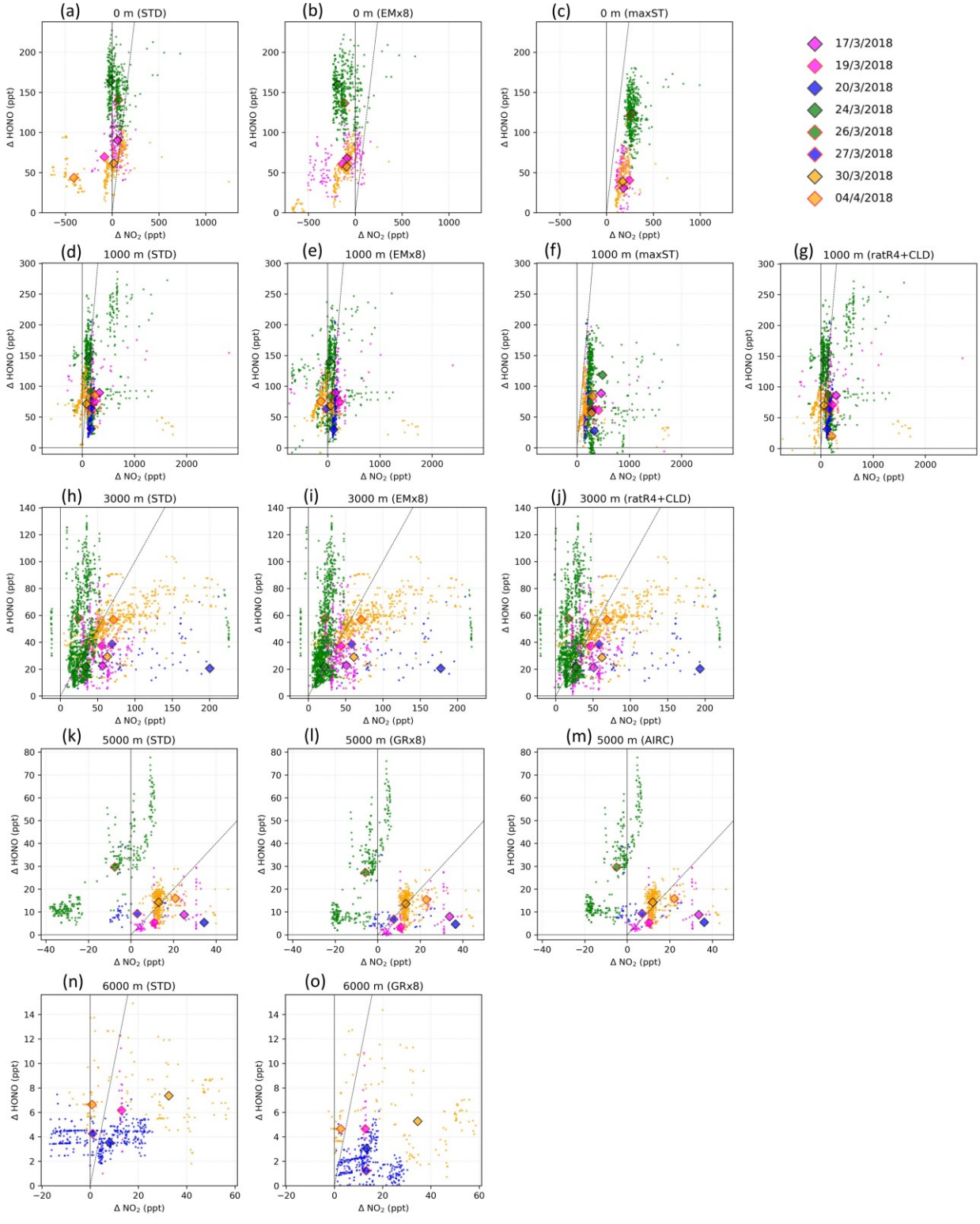

https://doi.org/10.5194/gmd-2021-385
Preprint. Discussion started: 3 December 2021

Geoscientific Model Development Discussions

Figure 9: Discrepancies of measurement and simulations for HONO (Δ_{HONO}) compared to that for NO_2 (Δ_{NO2}). Only results from STD (first column) and helpful sensitivity cases (second, third, and fourth columns) are plotted, scaled similar to the first column. Top of each panel shows the altitude range (0, 1000, 3000, 5000, 6000 m ± 500 m) and name of the sensitivity case. For each panel, small points represent discrepancies distribution (OBS – STD) or (OBS – sensitivity runs). Diamonds with black or red outlines mark the median point of the distribution. Colours represent flight cruises: Taiwan – South Korea – Taiwan on 17/3 and 19/3 (magenta), Taiwan – South Korea on 24/3 and 26/3 (green), Taiwan – Philippines on 20/3 and 27/3 (blue), and Taiwan – Japan on 30/4 and 4/4 (orange). Vertical, horizontal, and diagonal lines are $\Delta_{NO2} = 0$, $\Delta_{HONO} = 0$, $\Delta_{NO2} = \Delta_{HONO}$, respectively.

3.2 HONO's global distribution and effects

3.2.1 Global HONO distribution and budgets

This section sheds the light on the global HONO distribution computed for the STD case. The surface HONO concentration is peaked over the geographical region that embraces China, with seasonal mean levels up to 2.8 ppbv during summer and 7.8 ppbv during winter (Figure 10(a,b)). The winter peak agrees with observations for a large industrial region in the Yangtze River Delta of China (Zheng et al., 2020). The high concentrations of HONO are also identified in other industrial regional clusters: Northeast America (seasonal mean up to 0.5–1 ppbv), India (up to 1–3 ppbv), forest regions, especially the extra-tropic evergreen forest in Europe (up to 1–3 ppbv), and Africa (up to 0.5–1 ppbv). Over the ocean, HONO levels remain at 10–30 pptv in the coastal regions and below 10 pptv far off the coast. The simulated HONO distribution is in line with a previous study (Elshorbany et al., 2012) despite the peaks over polluted Chinese areas are markedly higher in our model (tenfold) The overestimation associated with the soot uptake in our model has been previously neglected. The highest HONO concentrations (10–30 pptv) in the free troposphere (at 2500 m) were simulated over Africa's biomass burning region during wet months (JJA) (Figure 10(c,d)), which could arise due to the NO_2 uptake on aerosols, originated from this wildfire source.

In the model, HRs and EM are the main contributors to HONO at the surface layer (Figure 11) by providing efficient HONO formation and promoting gas reaction (R2). Of the various surfaces, provided for HRs in our model, liquid/ice cloud particle surfaces are supposed to catalyze significant photochemical effects in remote regions. This phenomenon has not been previously addressed in detail. The uptake of liquid/ice cloud particles either increases HONO formation via (R4) for the tropical and southern oceans or reduce it via (R6) along 60 °S in DJF and Artic in JJA (Figure 11(a,b)). Besides cloud particles, HRs on aqueous aerosols also produce HONO in a continental atmosphere rich in sulfate, dust, and soot particles (Figure 11(c,d)). EM included in the model has sharply increased the HONO level over deserts (Sahara, Arabian), grasslands (South Africa, South America), boreal, and agricultural land (West Europe, Australia). This finding agrees well with another study, based on spaceborne observations for HONO in wildfire plumes (Theys et al., 2020), and along ship tracks in the marine boundary layer (Figure 11(e,f)).

Table 8 summarizes the global sources and sinks of tropospheric HONO quantified by CHASER. The simulations indicate that GRs contribute only for 11% of the HONO net production. More significant HONO is produced by HRs and EM (contribute to 63% and 26% HONO net production, respectively). The pyrogenic HONO emission estimated in this study might be underestimated as $HONO/NO_x$ emission ratio could be enhanced by up to 1 at extratropic evergreen forests (universally 0.1 in this study (STD)) (Theys et al., 2020). For large metropolitan areas such as those in China, HRs and EM

https://doi.org/10.5194/gmd-2021-385
Preprint. Discussion started: 3 December 2021

Geoscientific Model Development Discussions

have also been reported as the two most significant contributors to HONO formation, at ~59% and 26–29%, respectively (Li et al., 2011; Zhang et al., 2016). Of the various surfaces provided for HRs, aerosols represent more effective HONO formation site (~51.2%), compared with ice and clouds as they are contributing only 11.8% to HONO production. Moreover, the HONO loss through photolysis (R1) and (R3) is equivalent to its uptake onto the particles (R6). In equilibrium, the tropospheric abundance of HONO averaged of the globe is estimated to be 1.4 TgN in our model.

Table 8: Global sources and sinks of tropospheric HONO calculated by CHASER. Data from 2011.

Sources (TgN/yr)	35.17	Sinks (TgN/yr)	33.77	Net productions (TgN/yr)	1.40
P_{GR}	13.24	L_{GR}	13.09	GRs	0.15(11%)
P_{HR}	15.31	L_{HR}	14.43	HRs	0.88 (63%)
$P_{HR(cld)}$	9.57	$L_{HR(cld)}$	9.40	HRs(cld)	0.17 (11.8%)
$P_{HR(ae)}$	5.74	$L_{HR(ae)}$	5.03	HRs(ae)	0.72 (51.2%)
S_{EM}	6.62	L_{EM}	6.25	EM	0.37 (26%)

P denotes chemical production, S denotes source (emission + chemical production), and L denotes loss. The numbers in parentheses represent the portion of each pathway to the total HONO net production.

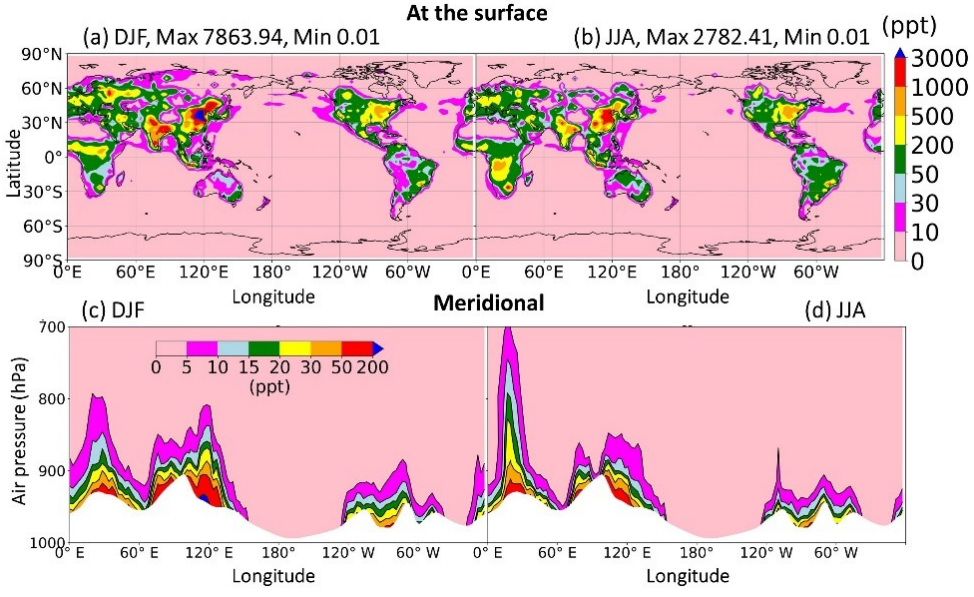

Figure 10: Distribution of HONO levels at the surface (a-b) and meridional mean (c-d).

https://doi.org/10.5194/gmd-2021-385
Preprint. Discussion started: 3 December 2021

Geoscientific Model Development Discussions

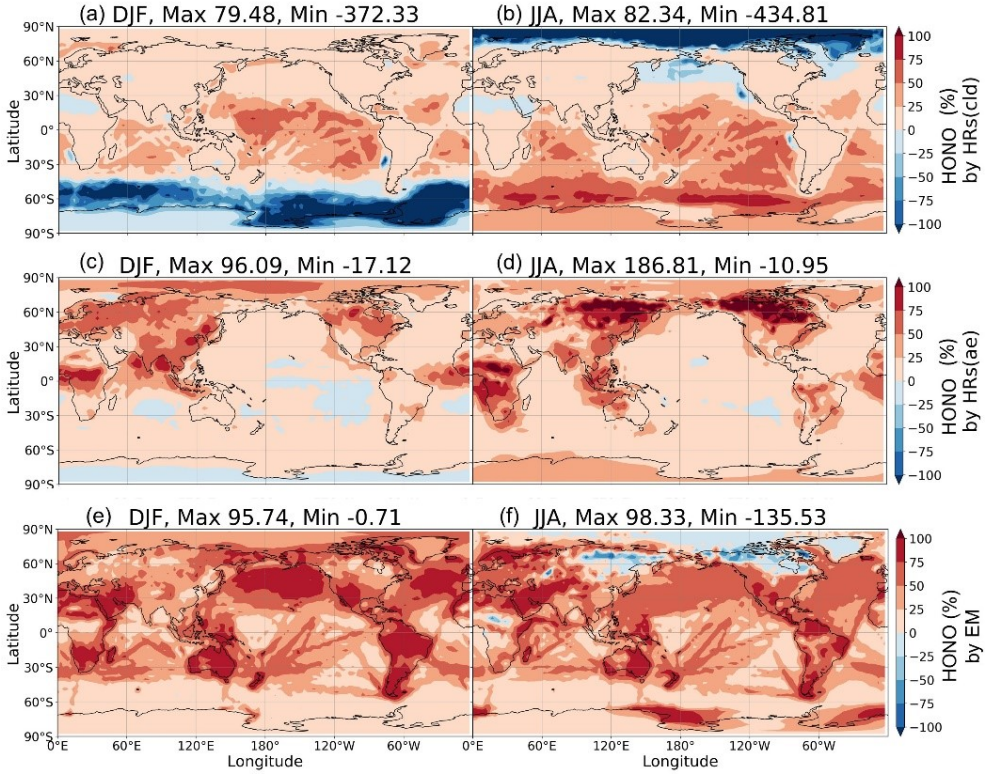

605 **Figure 11: Contribution of HRs and EM to surface HONO concentrations. Contributions of HRs onto ice and clouds (a, b), HRs onto aerosols (c, d), EM (e, f) in DJF (left) and JJA (right) are plotted. Each contribution is determined by the difference of HONO in two simulations: (a, b): GR+HR(cld) and GR, (c, d): GR+HR and GR+HR(cld), (e, f): STD and GR+HR, divide by HONO in STD case. The maximum and minimum values are out-scaled hence displayed at the tops of each panel.**

3.2.2 Implication of HONO on the tropospheric photochemistry

610 In this section, the global impact of HONO photochemistry is elucidated. To this end, Table 8 summarizes the HONO budget and the contribution of each pathway to the HONO photochemical cycle. Table 9 describes its consequences for the lifetime of CH_4, and the budgets of NO_x, O_3, and CO. The gaseous reactions of HONO tend to increase the abundance of NO_x, O_3, and CO (+1.01%, +0.15%, +0.44%, respectively) and CH_4 lifetime (+0.36%) in the troposphere. Without heterogeneous and direct emissions, the relatively low HONO formation by gaseous reactions (11% of the total net HONO production; Table 8) did not
615 cause any significant effects on NO_x, O_3, and CO in the troposphere.

Heterogeneous reactions that produce HONO are the most salient contributing factors to tropospheric chemistry, thereby, decreasing the tropospheric oxidizing capacity and increasing the CH_4 lifetime by 15% and CO abundance by 10%. HRs also reduces NO_x level by 23% and O_3 level by 6%, respectively (Table 9). The global HONO distribution from Figure 12 is mainly caused by the HR formation of HONO. Here, the reducing effects for NO_x levels, with consequences for OH and O_3 level
620 reductions by heterogeneous reactions, are significant at mid-to-high latitudes during summer. More specifically, in DJF along 60 °S and the Arctic and NP oceans during JJA, which amounted to about a -100% reduction in NO_x level at the surface (-60%

https://doi.org/10.5194/gmd-2021-385
Preprint. Discussion started: 3 December 2021


Geoscientific Model Development Discussions

in OH and -40% in O_3) (Figure 12(a-f): blue areas). These reductions in NO_x, OH, and O_3 levels extend up to 400 hPa at high N/S latitudes (Figure 12(k, l)). All these reduction effects for NO_x, OH, and O_3 levels are due to the removal of HONO on ice and cloud particles (R6) (Figure 11(a, b)). On one hand, it accelerates the conversion of NO_2 to HONO and ultimately strengthen its deposition by particulate nitrate (R4). On the other hand, HRs occurring on aerosol surfaces lead to increments in OH and O_3 near the surface of polluted regions during winter. These are the main contributors to the regional photochemical effects over China, Western Europe, and East U.S. regions in winter (up to -74% in NO_x, +1500% OH, +48% in O_3, Figure 12(a,c,e)). However, these increases of OH and O_3 levels are only accumulated in the surface layer (only small red areas at ~1000 hPa in Figure 12(i,m)). Compared to HRs on aerosol, HRs on clouds exhibit twofold effectiveness when reducing tropospheric NO_x level (-15% versus -8%) and cause threefold effects on the tropospheric oxidation capacity (+11.5% in CH_4 lifetime, -4.6% in O_3, +7% in CO), compared with HRs on aerosol (+3.5% CH_4 lifetime, -1.5% O_3, +2.6% CO) (Table 9).

Given the direct emissions of HONO (~10% of NO_x emission inventory), the surface NO_x, O_3, and OH concentrations are generally enhanced in the STD case compared to the GR+HR case. They induce the concentration modification for NO_x (+1.77%), O_3 (+0.97%), CO (-1.63%), and a significant reduction (-2.3%) in the CH_4 lifetime (Table 9). Remarkable enhancements for NO_x (up to +198%), OH (+243%), and O_3 (+24%) (Figure 12(b,d,f): red fields) were identified for the cropland and shrubland/forest regions in Australia, South America, and South Africa during JJA, and the boreal vegetation prevailing at mid-high latitudes in Europe, North America, and the polluted Chinese region in DJF (up to +748% OH) (Figure 12(a): red fields). NO_x and OH were elevated in these mid-latitude regions because of the enhanced HONO photolysis (R1) by the additional HONO source. However, OH, NO_x, and O_3 levels were reduced near the surface of the Northern Hemisphere's land during summer (up to -47% OH, -82% NO_x, and -15% O_3) (Figure 12(b,d,f)). The latter phenomenon is similar to the heterogeneous cloud effects for the high latitudes discussed above.

Overall, the inclusion of the three HONO processes (gas phase, aerosol and cloud uptakes, direct emission) causes -20% in NO_x, -5% in O_3, +8% in CO, and a significant increase of +13% CH_4 lifetime in the troposphere (Table 9). Figure 13 highlights the consequences of HO_x, NO_x, and O_3 for the Chinese and NP regions. NO_x level reduction accumulates in the Arctic and Antarctic during summer, especially over the NP ocean (reducing NO_x level by 60–90%, Figure 13(i)). These reductions in NO_2 and HONO concentrations are due to their uptake onto ice and clouds in these regions. However, these reducing effects cause further reductions in OH and O_3 levels for a larger part of the troposphere. As NO_x is essential in regulating O_3 and OH in the troposphere, a reduction of NO_x level increases the HO_2/OH ratio (due to the $HO_2 + NO \rightarrow OH + NO_2$ reaction), which restrains the formation of OH and ultimately of O_3. Thus, in summer, both OH and O_3 levels are drastically reduced over the NP region (35–67% for OH, 30–43% for O_3, Figure 13(g,k)), but CO level is increased by 18% in this region (Figure 12(h)).

The significant impacts of HONO photochemistry are especially relevant over Eastern China in winter, which may reduce NO_x level by 48–78% (Figure 12(c)) due to the uptake of NO_2 onto aqueous aerosols. At the surface, OH level is enormously increased as a result of HONO photolysis (R1), heterogeneous NO_2 conversions (R4, R5), and additional direct emissions (Figure 13(a,b)). The corresponding increase in O_3 level was only identified at the surface of the Beijing region during winter,

https://doi.org/10.5194/gmd-2021-385
Preprint. Discussion started: 3 December 2021

Geoscientific Model Development Discussions

with +28.8% caused by HRs on aerosols (Figure 13(e)). For Beijing with high NO_x emissions, VOC-limited O_3 chemistry is likely the driving mechanism (Liu et al., 2010). The vast increases in OH and O_3 levels over Beijing in winter are basically in line with the present knowledge of HONO photochemistry (e.g., Lu et al., 2018). Elshorbany et al. (2012) also reported an increase in OH ($2–5\times10^6$ molecules cm^{-3}) and O_3 (0.3–0.5 ppbv) concentrations over polluted regions in China during winter. Compared with Elshorbany's work, the increases in OH and O_3 concentrations in our model are higher due to the different HONO mechanisms applied in the two models, simply an averaged $HONO/NO_x$ ratio (0.02) in their model. In particular, our newly added heterogeneous reactions on cloud particles (R4) caused significant reductions in OH, NO_x, and O_3 levels in the NP region during summer, which their model does not cover. The overall reductions in tropospheric oxidizing capacity due to HONO photochemistry are in line with the expected response to heterogeneous processes (Liao et al., 2003; Martin et al., 2003) and agree with those previously reported for other HRs (HO_2, N_2O_5, and RO_2) previously reported (Ha et al., 2021) (Table 9). Our findings indicate that a global model without heterogeneous processes for HONO would neglect the significant changes in OH and O_3 concentrations in remote areas and, thus, will underestimate the potential effects in polluted regions.

Table 9: CH_4 lifetime and tropospheric abundances for NO_x, O_3, CO and the changes by HONO chemistry

Simulation ID	CH_4 lifetime (yr)	Abundances of tropospheric		
		NO_x (TgN)	O_3 (TgO_3)	CO (TgCO)
OLD	9.09	0.119	408.79	327.20
GR	9.12	0.120	409.38	328.65
GR+HR	10.49	0.092	384.25	359.90
GR+HR(cld)	10.17	0.102	390.46	351.53
STD	10.28	0.094	388.21	354.57
Effects		Changes (%)		
by GRs:	+0.36	+1.01	+0.15	+0.44
by HRs:	+14.99	-23.19	-6.15	+9.55
by HR(cld):	+11.52	-15.28	-4.63	+6.99
by HR(ae):	+3.47	-7.91	-1.52	+2.56
by EM:	-2.30	+1.77	+0.97	-1.63
Total:	+13.05	-20.40	-5.03	+8.36
by HRs(N_2O_5,HO_2,RO_2) (Ha et al., 2021)	+5.7	-3.87	-2.91	+3.43

https://doi.org/10.5194/gmd-2021-385
Preprint. Discussion started: 3 December 2021

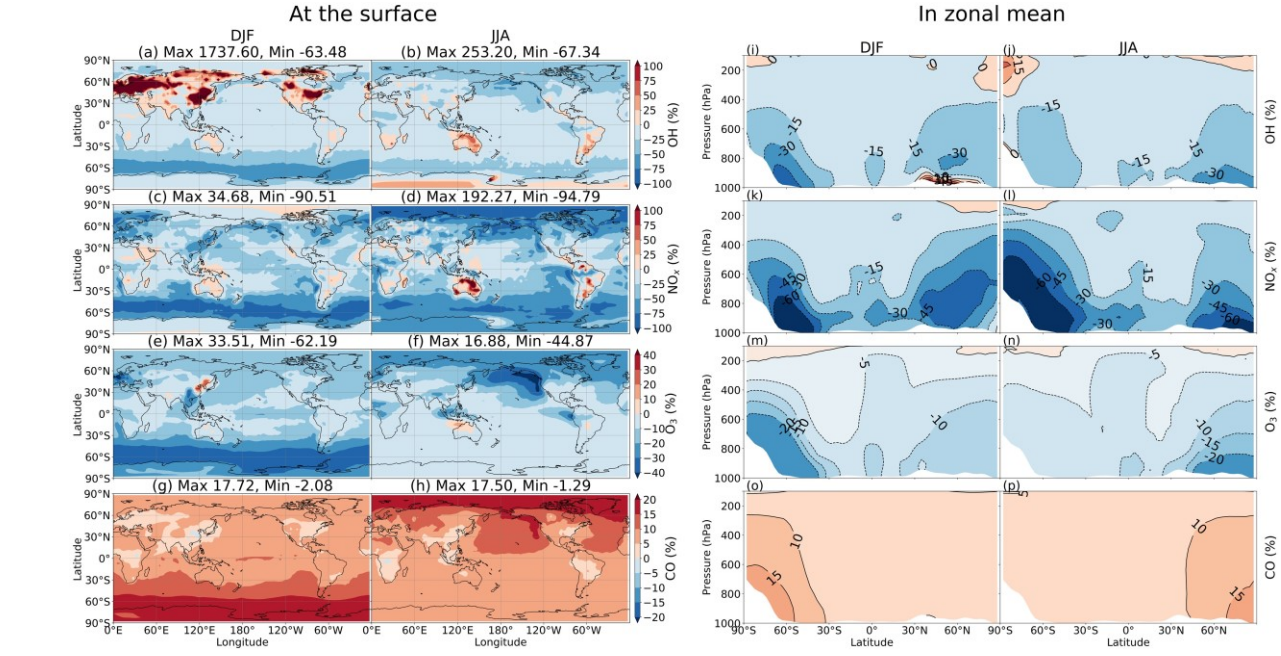

Figure 12: Effects of the HONO photochemistry on the tropospheric oxidants OH (first row of panels), NOx (second row of panels), O3 (third row of panels) and (CO last row of panels). Effects at near the surface (a-h) and zonal means (i-p) are shown.

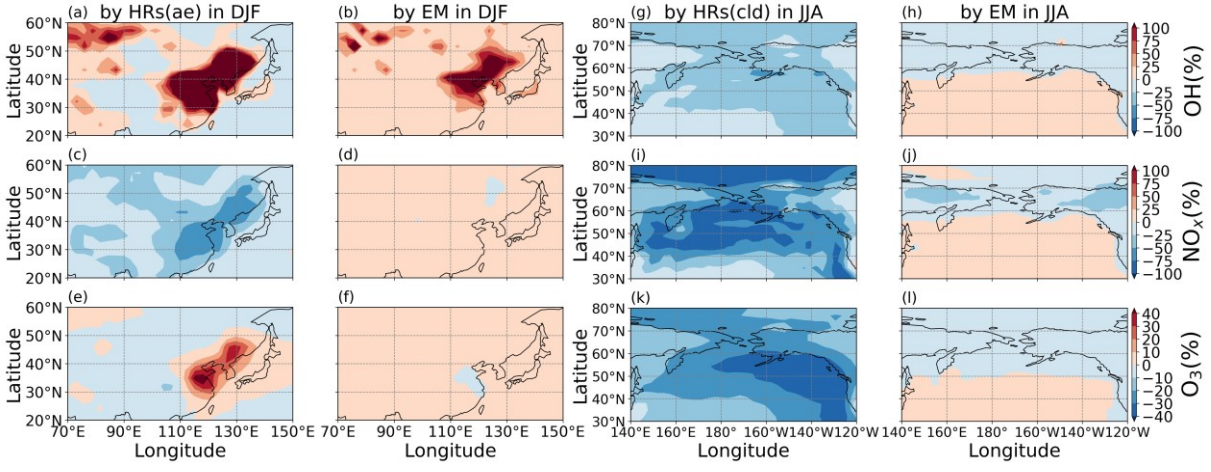

Figure 13: Effects of HONO photochemistry for the surface layer, for OH (upper panels), NO_x (middle panels), and O_3 (lower panels) over northeastern China region in DJF (a-f) and NP region in JJA (g-l) from dominant pathways of HONO by heterogeneous reactions of aerosols (1st column heterogeneous reactions ice and clouds (3rd column) and direct HONO emission (2nd and 4th columns).

4 Conclusion

The HONO photochemical processes, including (a) the gas-phase reaction involving HONO, (b) direct HONO emission from combustion and soil crust, as well as (c) heterogeneous processes involving HONO; all were added to the chemistry-climate

https://doi.org/10.5194/gmd-2021-385
Preprint. Discussion started: 3 December 2021


Geoscientific Model Development Discussions

model (CHASER) for the first time by this study. We found that the model biases are reduced against the EANET/EMEP stationary observations for $PM_{2.5}$, NO_3 components, O_3, and CO concentrations when the HONO photochemistry is included. The overestimations of OMI-based TCO by simulations are mostly reduced by the HONO inclusion given its reducing effects for O_3, which notably includes the geographical region that embraces China. Although the simulation underestimations of surface O_3 in the NP region is associated with the inconsistent surface deposition or vertical fluxes (c.f. from the stratosphere) becoming stronger, the model still stands out with NO_2, OH, and CO improvements in this region, compared with the observations made during *Mirai* and ATom1. We also compared the measurements during the EMeRGe flights off the coast region of East Asia and discerned good agreement between the measured and calculated NO_2, O_3, and CO profiles. However, the influence of the Chinese river delta regions is not reflected in the model, as the large reductions in air masses affected by land emissions were identified.

In the model, the tropospheric abundance for HONO is 1.4 TgN and is made by 26% from the direct emission and 63% by HRs, in which HRs on clouds cause 11.8% and HRs on aerosols cause 51.2%. The HONO concentrations over the continents range from 30 ppt to 7 ppb and are maximized due to HRs over the eastern China during winter. Only 5–10 ppt of HONO can be transported up to an altitude of ~2000 m, thereby, indicating that its impacts remain mainly in the planetary boundary layer. We argue that these simulated HONOs may underestimate the actual concentrations off-coast of eastern Asia in spring 2018. The unknown daytime HONO concentrations of up to 200 ppt measured in the boundary layer and free troposphere during the EMeRGe campaign are not reproduced well by the model, possibly due to the small concentrations of NO_2, O_3, and CO in the model. Therefore, a further improvement of the model performance for the HONO photochemistry requires (1) the revised model's emission inventory with the emission sources of NO_x and CO from South-Eastern and Eastern Asia, (2) the lighting-related NO_x module is upgraded, and (3) the vertical mixing and downward fluxes from the stratosphere to be elaborated. Higher uptake coefficients for aerosols near the surface and in the middle troposphere and on cloud droplets at ~1000 m could also produce more HONO and, therefore, alleviate the model discrepancies. The direct emissions of HONO from aircraft traffic may be an efficient local HONO source during the daytime. Moreover, the potential presence of aviation-originated aerosols in the middle troposphere for NO_2 conversion should be further investigated. One or more renoxification mechanisms converting HNO_3 into NO_x should be added to the model to overcome the observed and simulated NO_x seasonality mismatches. Shifting the product ratio towards more HONO and less HNO_3 in reaction R4 can also provide more HONO and can mitigate the deteriorated representation of NO_x seasonality. The sensitivity tests also suggest that more robust aerosol processing in polluted areas and less HNO_3 product in R4 can further reduce O_3 level in summer, therefore, reducing the bias with regards to measurements. Besides that, both the diurnal and nocturnal HONO concentrations can be enhanced.

Of the three HONO sources, HRs produced the most prominent effects on the tropospheric photochemistry: reducing OH, NO_x, O_3, and increasing CO levels in the troposphere, leading to a +13.05% longer CH_4 lifetime, and -20.4% less NO_x, -5.03% less O_3, and an increased CO (+8.36%) abundance. In winter near the surface, gas-phase reactions involving HONO and NO_2 conversions on soot induce significant photochemical effects over eastern Chinese with changes of -60% in NO_x, +1700% in OH, +33% in O_3. During summer, HRs on ice and cloud particles could cause significant changes of -67% in OH, -45% in O_3,

https://doi.org/10.5194/gmd-2021-385
Preprint. Discussion started: 3 December 2021

-75% in NO_x, and +17% in CO in the NP region. Albeit the more significant contribution of heterogeneous reactions to aerosols, the net HONO production, heterogeneous processes involving ice and cloud particles are more significant on a global scale. We found that the HONO chemistry, including the heterogeneous processes on cloud particles, can reduce the troposphere's oxidizing capacity on a global scale. It should be underlined that this finding is rather unexpected and is in contrast with the increasing oxidation capacity, previously reported for polluted areas. This new finding may also affect climate change mechanisms and, as a result, may influence its mitigation policies. Overall, our results prove that a global model without heterogeneous HONO formation, especially HRs on cloud particles, can bias the overall impacts of HONO on tropospheric photochemistry as it neglects the photochemical effects of HONO in remote areas and underestimates them in polluted regions. Notably, these photochemical effects of the HONO photochemistry on the tropospheric oxidizing power can be dwindled in the case of shifting of (R4)'s product ratio toward more HONO and less HNO_3 production, thereby, causing a reduction in the CH_4 lifetime from +13.1% to +5.6%.

Code availability

The CHASER V4.0' source code and input data to recreate this work's results can be acquired from the repository at https://doi.org/10.5281/zenodo.4153452 (Ha et al., 2020).

Data availability

The primary data from *R/V Mirai* cruises for the period 2015–2017 are available from http://www.godac.jamstec.go.jp/darwin/e (last access: 30 September 2021). Due to a recent data security incident, the data owner (JAMSTEC) is suspending public access to this dataset. For any inquiries, please send email to yugo@jamstec.go.jp. The data collected by HALO aircraft during the EMeRGe campaign are listed on https://www.iup.uni-bremen.de/emerge/home/halo_payload.html and can be acquired via email to Klaus.Pfeilsticker@iup.uni-heidelberg.de.

Author contribution

HP composed all simulations and text. SK has the model code and supervised the findings of this study. KY and TF provided *R/V Mirai* ship data. HM, BS, and KP provided EMeRGe-Asia data. All authors have equally contributed to the discussion provided within the manuscript, and post-writing formatting and revisions.

Competing interests

The authors declare that they have no conflicts of interest.

https://doi.org/10.5194/gmd-2021-385
Preprint. Discussion started: 3 December 2021


Geoscientific Model Development Discussions

Acknowledgements

We are grateful to the NASA scientists and staff for providing ATom data (https://espo.nasa.gov/atom/content/ATom) and OMI data (https://daac.gsfc.nasa.gov/). The simulations were completed using a supercomputer (NEC SX-Ace and SX-Aurora TSUBASA) at NIES Japan. The surface observational data for model validation were obtained from the monitoring networks EANET (https://www.eanet.asia/) and EMEP (https://www.emep.int/).

Financial support

This research was supported by the Global Environment Research Fund (S–12 and S–20) of the Ministry of the Environment (MOE), Japan, and JSPS KAKENHI Grant Numbers: JP20H04320, JP19H05669, and JP19H04235. The study was also funded by the German Research Foundation (Deutsche Forschungsgemeinschaft; DFG) HALO-SPP 1294. The contributions from BS and KP were supported via the DFG grants PF 384/16, PF 384/17 und PF 384/19.

https://doi.org/10.5194/gmd-2021-385
Preprint. Discussion started: 3 December 2021


Geoscientific Model Development Discussions

References

Acker, K., Febo, A., Trick, S., Perrino, C., Bruno, P., Wiesen, P., Moller, D., Wieprecht, W., Auel, R., Giusto, M., Geyer, A., Platt, U., Allegrini, I.: Nitrous acid in the urban area of Rome. Atmospheric Environment. 40(17): 3123–3133, doi: 10.1016/j.atmosenv.2006.01.028, 2006.

Acker, K., Moller, D., Wierecht, W., Auel, R., KalaX, D., Tscherwenka, W.: Nitrous and nitric acid measurements inside and outside of clouds at Mt. Brocken, Water, Air and Soil Pollution. 130: 331–336, 2001.

Akimoto, H., Nagashima, T., Li, J., Fu, J. S., Ji, D., Tan, J., Wang, Z.: Comparison of surface ozone simulation among selected regional models in MICS-Asia III – effects of chemistry and vertical transport for the causes of difference, Atmos. Chem. Phys. 19: 603-615, doi: 10.5194/acp-19-603-2019, 2019.

Al-Abadleh, H. A., Grassian, V. H.: Heterogeneous reaction of NO_2 on hexane soot: A Knudsen cell and FT-IR study, J. Phys. Chem. A, 104, 11926-11933, 2000.

Ammann, M., Kalberer, M., Jost, D. T., Tobler, L., Rossler, E., Piguet, D., Gaggeler, H. W., Baltensperger, U.: Heterogeneous production of nitrous acid on soot in polluted air masses, Nature, 395, 157-160, 1998.

Ammann, M., Kalberer, M., Tabor, K., Tobler, K., Zellweger, C., Weingartner, E., Nyeki, S., Parrat, Y., Li, F., Piguet, D., Rossler, E., Jost, D. T., Gaggeler, H. W., Baltensperger, U.: Proc. 7th Euro. Symp. on Physico-Chem. Behav. of Atmos. Poll., 1996.

Andrés Hernández, M. D., Hilboll, A., Ziereis, H., Förster, E., Krüger, O. O., Kaiser, K., Schneider, J., Barnaba, F., Vrekoussis, M., Schmidt, J., Huntrieser, H., Blechschmidt, A.-M., George, M., Nenakhov, V., Klausner, T., Holanda, B. A., Wolf, J., Eirenschmalz, L., Krebsbach, M., Pöhlker, M. L., Hedegaard, A. B., Mei, L., Pfeilsticker, K., Liu, Y., Koppmann, R., Schlager, H., Bohn, B., Schumann, U., Richter, A., Schreiner, B., Sauer, D., Baumann, R., Mertens, M., Jöckel, P., Kilian, M., Stratmann, G., Pöhlker, C., Campanelli, M., Pandolfi, M., Sicard, M., Gomez-Amo, J. L., Pujadas, M., Bigge, K., Kluge, F., Schwarz, A., Daskalakis, N., Walter, D., Zahn, A., Pöschl, U., Bönisch, H., Borrmann, S., Platt, U., and Burrows, J. P.: Overview: On the transport and transformation of pollutants in the outflow of major population centres – observational data from the EMeRGe European intensive operational period in summer 2017, Atmos. Chem. Phys. Discuss. [preprint], doi: 10.5194/acp-2021-500, in review, 2021.

Appel, B. R., Winer, A. M., Tokiwa, Y., Biermann, H. W.: Comparison of atmospheric nitrous acid measurements by annular denuder and differential optical absorption systems, Atmos. EnViron., 24A (3), 611-616, 1990.

Arens, F., Gutzwiller, L., Baltensperger, U., Gaggeler, H., Ammann, M.: Heterogeneous reaction of NO_2 on diesel soot particles. Environ. Sci. Technol., 35, 2191-2199, 2001.

Aumont, B., Chervier, F., Laval, S.: Contribution of HONO sources to the $NO_x/HO_x/O_3$ chemistry in the polluted boundary layer. Atmos. Environ. 37, 487–498, 2003.

Benedict, K. B., McFall, A. S., and Anastasio, C.: Quantum Yield of Nitrite from the Photolysis of Aqueous Nitrate above 300 nm, Environ. Sci. Technol. 2017, 51, 4387−4395, doi: 10.1021/acs.est.6b06370, 2017.

https://doi.org/10.5194/gmd-2021-385
Preprint. Discussion started: 3 December 2021

Benedict, K. B., and Anastasio, C., Quantum Yields of Nitrite (NO_2^-) from the Photolysis of Nitrate (NO_3^-) in Ice at 313 nm, J. Phys. Chem. A 2017, 121, 8474−8483, doi: 10.1021/acs.jpca.7b08839, 2017.

Bongartz, A., Kames, J., Schurath, U., George, Ch., Mirabel, Ph., Ponche, J. L. J.: Experimental determination of HONO mass accommodation coefficients using two different techniques, Atmos. Chem., 18, 149-169, 1994.

Brune, W. H., McFarland, P. J., Bruning, E., Waugh, S., MacGorman, D., Miller, D. O., Jenkins, J. M., Ren, X., Mao, J., Peischl, J.: Extreme oxidant amounts produced by lightning in storm clouds, Science 372, 711–715, 2021.

Burkholder, J. B., Mellouki, A., Talukdar, R.: Ravishankara, A. R.: Rate coefficients for the reaction of OH with HONO between 298 and 373 K, Int. J. Chem. Kinet., 24, 711-725, 1992.

Burkholder, J. B., Sander, S. P., Abbatt, J., Barker, J. R., Huie, R. E., Kolb, C. E., Kurylo, M. J., Orkin, V. L., Wilmouth, D. M., and Wine, P. H.: Chemical Kinetics and Photochemical Data for Use in Atmospheric Studies, Evaluation No. 18, JPL Publication 15-10, Jet Propulsion Laboratory, Pasadena, http://jpldataeval.jpl.nasa.gov, 2015.

Calvert, J.G., Yarwood, G., Dunker, A.M.: An evaluation of the mechanism of nitrous acid formation in the urban atmosphere, Research on Chemical Intermediates, 20, 463-502, 1994.

Cape, J. N., Hargreaves, K. J., Storeton-West, R., Fowler, D., Colvile, R. N., Choularton, T. W., Gallagher, M. W.: The contribution of HONO to rural NO_y chemistry as inferred from measurements of nitrite in orographic cloud, Atmos. Environ., 26A, 2301-2307, 1992.

Chu, L., Diao, G., Chu, L. T.: Heterogeneous Interaction and Reaction of HONO on Ice Films between 173 and 230 K, J. Phys. Chem. A, 104, 3150-3158, 2000.

Deutschmann, T., Beirle, S., Frieß, U., Grzegorski, M., Kern, C., Kritten, L., Platt, U., Prados-Roman, C., Puķīte, J., Wagner, T., Werner, B., and Pfeilsticker, K.: The Monte Carlo atmospheric radiative transfer model McArtim: Introduction and validation of Jacobians and 3D features, J. Quant. Spectrosc. Ra.: 112: 1119–1137, doi:10.1016/j.jqsrt.2010.12.009, 2011.

Elshorbany, Y. F., Kleffmann, J., Kurtenbach, R., Lissi, E., Rubio, M., Villena, G., Gramsch, E., Rickard, A. R., Pilling, M. J., Wiesen, P.: Seasonal dependence of the oxidation capacity of the city of Santiago de Chile, Atmos. Environ., 44, 5383–5394, 2010.

Elshorbany, Y. F., Steil, B., Bruhl, C., Lelieveld, J.: Impact of HONO on global atmospheric chemistry calculated with an empirical parameterization in the EMAC model, Atmos. Chem. Phys., 12, 9977–10000, 2012.

Febo, A., Perrino, C., Allegrini, I.: Measurement of nitrous acid in Milan, Italy, by DOAS and diffusion denuders, Atmos. EnViron., 30 (21), 3599-3609, 1996.

Fenter, F. F. and Rossi, M. J.: Heterogeneous Kinetics of HONO on H_2SO_4 Solutions and on Ice: Activation of HCl, J. Phys. Chem., 100, 13765-13775, 1996.

Finlayson-Pitts, B. J., Wingen, L. M., Sumner, A. L., Syomin, D., Ramazan, K. A.: The heterogeneous hydrolysis of NO_2 in laboratory systems and in outdoor and indoor atmospheres: An integrated mechanism, Phys. Chem. Chem. Phys., 5, 223–242, 2003.

https://doi.org/10.5194/gmd-2021-385
Preprint. Discussion started: 3 December 2021

George, C., Strekowski, R. S., Kleffmann, J., Stemmler, K., and Ammann, M.: Photoenhanced uptake of gaseous NO_2 on solid organic compounds: A photochemical source of HONO?, Faraday Discuss., 130, 195–210, 2005.

Gerecke, A., Thielmann, A., Gutzwiller, L., Rossi M. J.: The chemical kinetics of HONO formation resulting from heterogeneous interaction of NO_2 with flame soot, Geophysical Research Letters, 25(13), 1998.

Ha, P., Matsuda, R., Kanaya, Y., Taketani, F., and Sudo, K.: Effects of heterogeneous reactions on tropospheric chemistry: a global simulation with the chemistry-climate model CHASER V4.0, Geosci. Model Dev., 14, 1-29, doi: 10.5194/gmd-14-1-2021, 2021.

Harris, G.W., Carter, W.P.L., Winer, A.M., Pitts, J.N., Platt, U., Perner, D.: Observations of nitrous acid in the Los Angeles atmosphere and implications for predictions of ozone-precursor relationships, Environmental Science and Technology, 16, 414-419, 1982.

Harrison, R.M., Collins, G.M.: Measurements of reaction coefficients of NO_2 and HONO on aerosol particles, Journal of Atmospheric Chemistry, 30, 397-406, 1998.

Harrison, R.M., Kitto, N.: Evidence for a surface source of atmospheric nitrous acid, Atmospheric Environment, 28, 1089–1094, 1994.

Hayashi, K., Noguchi, I.: Indirect emission of nitrous acid from grasslands indicated by concentration gradients, Journal of Japan Society for Atmospheric Environment, 41(5), 279-287, 2006.

Hüneke, T., Aderhold, O-A., Bounin, J., Dorf, M., Gentry, E., Grossmann, K., Grooß, J-U., Hoor, P., Jöckel, P., Kenntner, M., Knapp, M., Knecht, M., Lörks, D., Ludmann, S., Matthes, S., Raecke, R., Reichert, M., Weimar, J., Werner, B., Zahn, A., Ziereis, H., Pfeilsticker, K.: The novel HALO mini-DOAS instrument: inferring trace gas concentrations from airborne UV/visible limb spectroscopy under all skies using the scaling method, Atmos. Meas. Tech., 10, 4209–4234, doi: 10.5194/amt-10-4209-2017, 2017.

Jacob, D. J.: Heterogeneous chemistry and tropospheric ozone, Atmospheric Environment, 34, Elsevier Science Ltd., 2000.

Jenkin, M. E., Cox, R. A.: Kinetics of the gas-phase reaction of OH with nitrous acid, Chem. Phys. Lett., 137, 548-552, 1987.

Jenkin, M. E., Cox, R.A., Williams, D.J.: Laboratory studies of the kinetics of formation of nitrous acid from the thermal reaction of nitrogen dioxide and water vapour, Atmospheric Environment, 22, 487-498, 1988.

Jorba, O., Dabdub, D., Blaszczak-Boxe, C., Pérez, C., Janjic, Z., Baldasano, J. M., Spada, M., Badia, A., Gonçalves, M.: Potential significance of photoexcited NO_2 on global air quality with the NMMB/BSC chemical transport model, J. Geophys. Res., 117, D13301, 2012.

Kalberer, M., Ammann, M., Arens, F., Gaggeler, H.W., Baltensperger, U.: Heterogeneous formation of nitrous acid (HNO_2) on soot aerosol particles. Journal Geophysical Research, 104 (D11), 13825–13832, 1999.

Kanaya, Y., Cao, R., Akimoto, H., Fukuda, M., Komazaki, Y., Yokouchi, Y., Koike, M., Tanimoto, H., Takegawa, N., and Kondo, Y.: Urban photochemistry in central Tokyo: 1. Observed and modeled OH and HO_2 radical concentrations during the winter and summer of 2004. J. Geophys. Res., 112, D21312, doi:10.1029/2007JD008670, 2007.

https://doi.org/10.5194/gmd-2021-385
Preprint. Discussion started: 3 December 2021


Geoscientific Model Development Discussions

Kanaya, Y., Miyazaki, K., Taketani, F., Miyakawa, T., Takashima, H., Komazaki, Y., Pan, X., Kato, S., Sudo, K., Sekiya, T., Inoue, J., Sato, K., and Oshima, K.: Ozone and carbon monoxide observations over open oceans on R/V *Mirai* from 67° S to 75° N during 2012 to 2017: testing global chemical reanalysis in terms of Arctic processes, low ozone levels at low latitudes, and pollution transport, Atmos. Chem. Phys., 19, 7233–7254, doi: 10.5194/acp-19-7233-2019, 2019.

Kerbrat, M., Huthwelker, T., Gaggeler, H. W., Ammann, M.: Interaction of Nitrous Acid with Polycrystalline Ice: Adsorption on the Surface and Diffusion into the Bulk, J. Phys. Chem. C, 114, 2208–2219, 2010.

Kessler, C. and Platt, U.: Nitrous acid in polluted air masses: sources and formation pathways. In Physicochemical Behaviour of Atmospheric Pollutan/s. Proc. 3rd Europ. Sump. Varese, Iralv (edited by Versino B. and Angdletti-G.j, pp. 412-422..Reidel, Doidrecht, 1984.

Kirchstetter, T. W., Harley, R. A., Littlejohn, D.: Measurement of Nitrous Acid in Motor Vehicle Exhaust, Environ. Sci. Technol., 30, 2843-2849, 1996.

Kleffman, J., Becker, K. H., Lackhoff, M., Wiesen, P.: Heterogeneous conversion of NO_2 on carbonaceous surfaces. Phys. Chem. Chem. Phys., 1, 5443-5450, 1999.

Kleffmann, J., Kurtenbacha, R., Lorzer, J., Wiesena, P., Kalthoffb, N., Vogelb, B., Vogel, H.: Measured and simulated vertical profiles of nitrous acid - Part I: Field measurements, Atmospheric Environment, 37, 2949–2955, 2003.

Kleffmann, J., Becker, K. H., Wiesen, P.: Heterogeneous NO_2 conversion processes on acid surfaces: possible atmospheric implications. Atmospheric Environment 32, 2721–2729, 1998.

Kleffmann, J. and Wiesen, P.: Heterogeneous conversion of NO_2 and NO on HNO_3 treated soot surfaces: atmospheric implications, Atmos. Chem. Phys., 5, 77–83, 2005.

Kluge, F., Hüneke, T., Knecht, M., Lichtenstern, M., Rotermund, M., Schlager, H., Schreiner, B., and Pfeilsticker, K.: Profiling of formaldehyde, glyoxal, methylglyoxal, and CO over the Amazon: normalized excess mixing ratios and related emission factors in biomass burning plumes, Atmos. Chem. Phys., 20, 12363–12389, https://doi.org/10.5194/acp-20-12363-2020, 2020.

Kurtenbach, R., Becker, K.H., Gomes, J.A.G., Kleffmann, J., Lorzer, J.C., Spittler, M., Wiesen, P., Ackermann, R., Geyer, A., Platt, U.: Investigations of emissions and heterogeneous formation of HONO in a road traffic tunnel, Atmospheric Environment, 35, 3385–3394, 2001.

Lammel, G., Cape, J. N.: Nitrous Acid and Nitrite in the Atmosphere, Chem. Soc. ReV., 361, 1996.

Lary, D. J., Lee, A.M., Toumi, R., Newchurch, M. J., Pirre, M., Renard, J. B.: Carbon aerosols and atmospheric photochemistry, Journal Of Geophysical Research, 102, D3, 3671-3682, 1997.

Lee, B. H., Santoni, G. W., Wood, E. C., Herndon, S. C., Miake-Lye, R. C., Zahniser, M. S., Wofsy, S. C., and Munger, J. W.: Measurements of Nitrous Acid in Commercial Aircraft Exhaust at the Alternative Aviation Fuel Experiment, Environ. Sci. Technol., dx.doi.org/10.1021/es200921t, 45, 7648–7654, 2011.

https://doi.org/10.5194/gmd-2021-385
Preprint. Discussion started: 3 December 2021

Lee, J. D., Whalley, L. K., Heard, D. E., Stone, D., Dunmore, R. E., Hamilton, J. F., Young, D. E., Allan, J. D., Laufs, S., Kleffmann, J.: Detailed budget analysis of HONO in central London reveals a missing daytime source. Atmos. Chem. Phys., 16, 2747–2764. doi: 10.5194/acp-16-2747-2016, 2016.

Li, Y., An, J., Min, M., Zhang, W., Wang, F., Xie, P.: Impacts of HONO sources on the air quality in Beijing, Tianjin and Hebei Province of China, Atmos. Environ., 45, 4735-4744, 2011.

Li, X., Brauers, T., Haseler, R., Bohn, B., Fuchs, H., Hofzumahaus, A., Holland, F., Lou, S., Lu, K. D., Rohrer, F. et al., Exploring the atmospheric chemistry of nitrous acid (HONO) at a rural site in Southern China, Atmos. Chem. Phys., 12, 1497–1513, 2012.

Li, X., Rohrer, F., Hofzumahaus, A., Brauers, T., Häseler, R., Bohn, B., Broch, S., Fuchs, H., Gomm, S., Holland, F., Jäger, J., Kaiser, J., Keutsch, F. N., Lohse, I., Lu, K., Tillmann, R., Wegener, R., Wolfe, G. M., Mentel, T. F., Kiendler-Scharr, A., Wahner, A., Missing Gas-Phase Source of HONO Inferred from Zeppelin Measurements in the Troposphere, Science, 344, 292 - 296, doi: 10.1126/science.1248999, 2014.

Li, J., Chen, X., Wang, Z., Du, H., Yang, W., Sun, Y., Hu, B., Li, J., Wang, W., Wang, T., Fu, P., Huang, H.: Radiative and heterogeneous chemical effects of aerosols on ozone and inorganic aerosols over East Asia, Science of the Total Environment, 622–623, 1327–1342, doi: 10.1016/j.scitotenv.2017.12.041, 2018.

Liao, H., Adams, P., Serena, H. C., Seinfeld, J. H., Mickley, L., Jacob, D. J.: Interactions between Tropospheric Chemistry and Aerosols in a Unified GCM Simulation, Journal of Geophysical Research, 108. 10.1029/2001JD001260, 2003.

Lin, M., Fiore, A. M., Cooper, O. R., Horowitz, L. W., Langford, A. O., Levy II, H., Johnson, B. J., Naik, V., Oltmans, S. J., and Senff, C. J.: Springtime high surface ozone events over the western United States: Quantifying the role of stratospheric intrusions, J. Geophys. Res., 117, D00V22, doi:10.1029/2012JD018151, 2012.

Liu, X.-H., Zhang Y., Xing J., Zhang Q., Wang K., Streets D.G., Jang C., Wang W.-X., Hao J.-M.: Understanding of regional air pollution over China using CMAQ, part II. Process analysis and sensitivity of ozone and particulate matter to precursor emissions, Atmospheric Environment, 44, 3719-3727, 2010.

Lu, X., Wang, Y., Li, J., Shen, L., Fung, C. H. J. : Evidence of heterogeneous HONO formation from aerosols and the regional photochemical impact of this HONO source, Environ. Res. Lett., 13, 114002, 2018.

Martin, R. V., Jacob, D. J., Yantosca, R. M., Chin, M., and Ginoux, P.: Global and regional decreases in tropospheric oxidants from photochemical effects of aerosols, J. Geophys. Res., 108(D3), 4097, 2003.

Meilinger, S. K., Karcher, B., and Peter, Th.: Microphysics and heterogeneous chemistry in aircraft plumes – high sensitivity on local meteorology and atmospheric composition, Atmos. Chem. Phys., 5, 533–545, 2005.

Mertes, S. and Wahner, A.: Uptake of nitrogen dioxide and nitrous acid on aqueous surfaces, Journal of Physical Chemistry, 99, 14000-14006, 1995.

Monge, M. E., D'Anna, B., Mazri, L., Giroir-Fendler, A., Ammann, M., Donaldson, D. J., and George, C.: Light changes the atmospheric reactivity of soot, Proc. Natl. Acad. Sci. U.S.A., 107(15), 6605–6609, 2010.

https://doi.org/10.5194/gmd-2021-385
Preprint. Discussion started: 3 December 2021

Morgenstern, O., Hegglin, M. I., Rozanov, E., O'Connor, F. M., Abraham, N. L., Akiyoshi, H., Archibald, A. T., Bekki, S., Butchart, N., Chipperfield, M. P., Deushi, M., Dhomse, S. S., Garcia, R. R., Hardiman, S. C., Horowitz, L. W., Jöckel, P., Josse, B., Kinnison, D., Lin, M., Mancini, E., Manyin, M. E., Marchand, M., Marécal, V., Michou, M., Oman, L. D., Pitari, G., Plummer, D. A., Revell, L. E., Saint-Martin, D., Schofield, R., Stenke, A., Stone, K., Sudo, K., Tanaka, T. Y., Tilmes, S., Yamashita, Y., Yoshida, K., and Zeng, G.: Review of the global models used within phase 1 of the Chemistry–Climate Model Initiative (CCMI), Geosci. Model Dev., 10, 639–671, doi:10.5194/gmd-10-639-2017, 2017.

Ndour, M., D'Anna, B., George, C., Ka, O., Balkanski, Y., Kleffmann, J., Stemmler, K., and Ammann, M.: Photoenhanced uptake of NO_2 on mineral dust: Laboratory experiments and model simulations, Geophys. Res. Lett., 35, L05812, 2008.

Notholt, J., Hjorth, J., and Raes, F.: Formation of HNO_2 on aerosol surfaces during foggy periods in the presence of NO and NO_2, Atmospheric Environment 26A, 211–217, 1992.

Oswald, R., Behrendt, T., Ermel, M., Wu, D., Su, H., Cheng, Y., Breuninger, C., Moravek, A., Mougin, E., Delon, C., Loubeta, B., Pommerening-Röserm, A., Sörgelu, M., Pöschlt, U., Hoffmannm, T., Andreaef, M. O., Meixnerand, F. X., Trebs, I.: HONO emissions from soil bacteria as a major source of atmospheric reactive nitrogen. Science, 341, 1233–1235, doi: 10.1126/science.1242266, 2013.

Perner, D. and Platt, U.: Detection of nitrous acid in the atmosphere by differential optical absorption, Geophysical Research Letters 6, 917–920, 1979.

Platt, U. and Perner, D.: Direct Measurements of Atmospheric CH_2O, HNO_2, O_3, NO_2, and SO_2 by Differential Optical Absorption in the Near UV, Journal of Geophysical Research, 85, C12, 7453-7458, 1980.

Platt, U., Stutz, J.: Differential Optical Absorption Spectroscopy, Springer, Berlin, Heidelberg, https://doi.org/10.1007/978-3-540-75776-4, 2008.

Porada, P., Tamm, A., Raggio, J., Cheng, Y., Kleidon, A., Pöschl, U., Weber, B.: Global NO and HONO emissions of biological soil crusts estimated by a process-based non-vascular vegetation model, Biogeosciences, 16, 2003-2031, 2019.

Reisinger, R.A.: Observations of HNO_2 in the polluted winter atmosphere: possible heterogeneous production on aerosols. Atmospheric Environment 34, 3865–3874, 2000.

Ren, X, Duin, D. van, Cazorla, M., Chen, S., Mao, J., Zhang, L., Brune, W. H., Flynn, J. H., Grossberg, N., Lefer, B. L., Rappenglück, B., Wong, K. W., Tsai, C., Stutz, J., Dibb, J. E., Jobson, B. T., Luke, W. T., Kelley, P.: Atmospheric oxidation chemistry and ozone production: Results from SHARP 2009 in Houston, Texas. J. Geophys. Res. Atmos.: 118: 5770–5780, doi:10.1002/jgrd.50342, 2013.

Romer, P. S., Wooldridge, P. J., Crounse, J. D., Kim, M. J., Wennberg, P. O., Dibb, J. E., Scheuer, E., Blake, D. R., Meinardi, S., Brosius, A. L., Thames, A. B., Miller, D. O., Brune, W. H., Hall, S. R., Ryerson, T. B., and Cohen, R. C.: Constraints on Aerosol Nitrate Photolysis as a Potential Source of HONO and NO_x, Environ. Sci. Technol. 2018, 52, 13738−13746, doi: 10.1021/acs.est.8b03861, 2018.

Rotermund, M. K., Bense, V., Chipperfield, M. P., Engel, A., Grooß, J.-U., Hoor, P., Hüneke, T., Keber, T., Kluge, F., Schreiner, B., Schuck, T., Vogel, B., Zahn, A., and Pfeilsticker, K.: Organic and inorganic bromine measurements around

https://doi.org/10.5194/gmd-2021-385
Preprint. Discussion started: 3 December 2021

the extratropical tropopause and lowermost stratosphere: insights into the transport pathways and total bromine, Atmos. Chem. Phys., 21, 15375–15407, doi: 10.5194/acp-21-15375-2021, 2021.

Rubio, M.A., Lissi, E., Villena, G.: Nitrite in rain and dew in Santiago city, Chile. Its possible impact on the early morning start of the photochemical smog. Atmospheric Environment 32, 293–297, 2002.

Saathoff, H., Naumann, K.-H., Riemer, N., Kamm, S., Mohler, O., Schurath, U., Vogel, H. and Vogel, B.: The loss of NO_2, HNO_3, NO_3/N_2O_5, and $HO_2/HOONO_2$ on soot aerosol: A chamber and modeling study, Geophysical Research Letters, 28, 10, 1957-1960, 2001.

Salgado-Muñoz, M. S. and Rossi, M. J.: Heterogeneous reactions of HNO_3 with flame soot generated under different combustion conditions. Reaction mechanism and kinetics. Phys. Chem. Chem. Phys., 4, 5110-5118, 2002.

Sakamaki, F., Hatakeyama, S., and Akimoto, H.: Formation of nitrous acid and nitric acid in the heterogeneous dark reaction of nitrogen dioxide and water vapour in smog chamber. J. them. Kinet. 15, 1013-1029, 1983.

Scharko, N. K., Berke, A. E., and Raff, J. D.: Release of Nitrous Acid and Nitrogen Dioxide from Nitrate Photolysis in Acidic Aqueous Solutions, Environ. Sci. Technol. 2014, 48, 11991−12001, dx.doi.org/10.1021/es503088x, 2014.

Schneider, J., Arnold, F., Btirger, V., Droste-Franke, B., Grimm, F., Kirchner, G., Klcmm, M., Stilp, T., Wohlfrom, K.-H., Siegmundand, P., and vanVelthoven, P. F. J.: Nitric acid (HNO_3) in the upper troposphere and lower stratosphereat midlatitudes: New results from aircraft-based massspeetrometric measurements. Journal Of Geophysical Research, 103, D19, 25,337-25,343, 1998.

Schwartz, S. E.: Mass-Transport Considerations Pertinent to Aqueous Phase Reactions of Gases in Liquid-Water Clouds: in Chemistry of Multiphase Atmospheric Systems, 415–471, Springer Berlin Heidelberg, 1986.

Sekiya, T., Miyazaki, K., Ogochi, K., Sudo, K., Takigawa, M.: Global high-resolution simulations of tropospheric nitrogen dioxide using CHASER V4.0. Geosci. Model Dev., 11, 959–988. doi: 10.5194/gmd-11-959-2018, 2018.

Sekiya, T. and Sudo. K.: Roles of transport and chemistry processes in global ozone change on interannual and multidecadal time scales. J. Geophys. Res.: 119, 4903–4921. doi: 10.1002/2013JD020838, 2014.

Stohl, A., Bonasoni, P., Cristofanelli, P., Collins, W., Feichter, J., Frank, A., Forster, C., Gerasopoulos, E., Ga¨ggeler, H., James, P., Kentarchos, T., Kromp-Kolb, H., Kru¨ger, B., Land, C., Meloen, J., Papayannis, A., Priller, A., Seibert, P., Sprenger, M., Roelofs, G. J., Scheel, H. E., Schnabel, C., Siegmund, P., Tobler, L., Trickl, T., Wernli, H., Wirth, V., Zanis, P., and Zerefos, C.: Stratosphere-troposphere exchange: A review, and what we have learned from STACCATO, J. Geophys. Res., 108(D12), 8516, doi:10.1029/2002JD002490, 2003.

Stutz, J., Alicke. B., Neftel. A.: Nitrous acid formation in the urban atmosphere: Gradient measurements of NO_2 and HONO over grass in Milan, Italy, Journal Geophysical Research, 107 (D22), 8192, 2002.

Stutz, J., Werner, B., Spolaor, M., Scalone, L., Festa, J., Tsai, C., Cheung, R., Colosimo, S. F., Tricoli, U., Raecke, R., Hossaini, R., Chipperfield, M. P., Feng, W., Gao, R.-S., Hintsa, E. J., Elkins, J. W., Moore, F. L., Daube, B., Pittman, J., Wofsy, S., Pfeilsticker, K.: A new Differential Optical Absorption Spectroscopy instrument to study atmospheric chemistry from a high-altitude unmanned aircraft, Atmos. Meas. Tech., 10, 1017–1042, doi:10.5194/amt-10-1017-2017, 2017.

Su, H., Cheng, Y., Oswald, R., Behrendt, T., Trebs, I., Meixner, F. X., Andreae, M. O., Cheng, P., Zhang, Y., and Pöschl, U., Soil Nitrite as a Source of Atmospheric HONO and OH Radicals, Science 333 (6049), 1616-1618, doi: 10.1126/science.1207687, 2011.

Sudo, K. and Akimoto, H.: Global source attribution of tropospheric ozone: Long-range transport from various source regions, J. Geophys. Res. Atmos.: 112: D12302. doi: 10.1029/2006JD007992, 2007.

Sudo, K., Takahashi, M., Kurokawa, J. I., and Akimoto, H.: CHASER: A global chemical model of the troposphere 1. Model description. J. Geophys. Res. Atmos.: 107: 4339. doi: 10.1029/2001JD001113, 2002.

Tan, Z., Fuchs, H., Lu, K., Hofzumahaus, A., Bohn, B., Broch, S., Dong, H., Gomm, S., Häseler, R., He, L., Holland, F., Li, X., Liu, Y., Lu, S., Rohrer, F., Shao, M., Wang, B., Wang, M., Wu, Y., Zeng, L., Zhang, Y., Wahner, A., Zhang, Y.: Radical chemistry at a rural site (Wangdu) in the North China Plain: observation and model calculations of OH, HO_2 and RO_2 radicals. Atmos. Chem. Phys., 17, 663–690. doi:10.5194/acp-17-663-2017, 2017.

Theys, N., Volkamer, R., Müller, J.-F., Zarzana, K. J., Kille, N., Clarisse, L., De Smedt, I., Lerot, C., Finkenzeller, H., Hendrick, F., Koenig, T. K., Lee, C. F., Knote, C., Yu, H. and Roozendael, M. V., Global nitrous acid emissions and levels of regional oxidants enhanced by wildfires, Nature geoscience, 13, 681–686, doi: 10.1038/s41561-020-0637-7, 2020.

Thornton, J. A., Jaeglé, L., and McNeill, V. F.: Assessing known pathways for HO_2 loss in aqueous atmospheric aerosols: Regional and global impacts on tropospheric oxidants. J. Geophys. Res. Atmos., 2008.

Trickl, T., Vogelmann, H., Giehl, H., Scheel, H.-E., Sprenger, M., and Stohl, A.: How stratospheric are deep stratospheric intrusions?, Atmos. Chem. Phys., 14, 9941–9961, doi:10.5194/acp-14-9941-2014, 2014.

VandenBoer, T. C., Brown, S. S., Murphy, J. G., Keene, W. C., Young, C. J., Pszenny, A. A. P., Kim, S., Warneke, C., de Gouw, J. A., Maben, J. R., Wagner, N. L., Riedel, T. P., Thornton, J. A., Wolfe, D. E., Dubé, W. P., Öztürk, F., Brock, C. A., Grossberg, N., Lefer, B., Lerner, B., Middlebrook, A. M., and Roberts, J. M.: Understanding the role of the ground surface in HONO vertical structure: High resolution vertical profiles during NACHTT-11, J. Geophys. Res. Atmos., 118, 10,155–10,171, doi:10.1002/jgrd.50721, 2013.

Watanabe, S., Hajima, T., Sudo, K., Nagashima, T., Takemura, T., Okajima, H., Nozawa, T., Kawase, H., Abe, M., Yokohata, T., Ise, T., Sato, H., Kato, E., Takata, K., Emori, S., and Kawamiya, M.: MIROC-ESM 2010: model description and basic results of CMIP5-20c3m experiments, Geosci. Model Dev., 4, 845–872, doi:10.5194/gmd-4-845-2011, 2011.

Werner, B., Stutz, J., Spolaor, M., Scalone, L., Raecke, R., Festa, J., Colosimo, S. F., Cheung, R., Tsai, C., Hossaini, R., Chipperfield, M. P., Taverna, G. S., Feng, W., Elkins, J. W., Fahey, D. W., Gao, R.-S., Hintsa, E. J., Thornberry, T. D., Moore, F. L., Navarro, M. A., Atlas, E., Daube, B. C., Pittman, J., Wofsy, S., and Pfeilsticker, K.: Probing the subtropical lowermost stratosphere and the tropical upper troposphere and tropopause layer for inorganic bromine, Atmos. Chem. Phys., 17, 1161–1186, doi: 10.5194/acp-17-1161-2017, 2017.

Winer, A. M. and Biermann, H. W.: Long pathlength differential optical absorption spectroscopy (DOAS) measurements of gaseous HONO, NO_2 and HCHO in the California South Coast air basin, Res. Chem. Intermed., 20, 423-445, 1994.

https://doi.org/10.5194/gmd-2021-385
Preprint. Discussion started: 3 December 2021

Xue, C., Ye, C., Kleffmann, J., Zhang, C., Catoire, V., Bao, F., Mellouki, A., Xue, L., Chen, J., Lu, K., Zhao, Y., Liu, H., Guo, Z., and Mu, Y.: Atmospheric Measurements at the Foot and the Summit of Mt. Tai – Part I: HONO Formation and Its Role in the Oxidizing Capacity of the Upper Boundary Layer, Atmos. Chem. Phys. Discuss. [preprint], https://doi.org/10.5194/acp-2021-529, in review, 2021a.

Xue, C., Ye, C., Kleffmann, J., Zhang, W., He, X., Liu, P., Zhang, C., Zhao, X., Liu, C., Ma, Z., Liu, J., Wang, J., Lu, K., Catoire, V., Mellouki, A., and Mu, Y.: Atmospheric Measurements at the Foot and the Summit of Mt. Tai – Part II: HONO Budget and Radical (ROx + NO3) Chemistry in the Lower Boundary Layer, Atmos. Chem. Phys. Discuss. [preprint], https://doi.org/10.5194/acp-2021-531, in review, 2021b.

Xue, C., Zhang, C., Ye, C., Liu, P., Catoire, V., Krysztofiak, G., Chen, H., HONO Budget and Its Role in Nitrate Formation in the Rural North China Plain, Environmental Science & Technology, 54, Nr. 18, 11048–57, doi: 10.1021/acs.est.0c01832, 2020.

Ye, C., Zhou, X., Pu, D., Stutz, J., Festa, J., Spolaor, M., Tsai, C., Cantrell, C., Mauldin III, R. L., Weinheimer, A., Hornbrook, R. S., Apel, E. C., Guenther, A., Kaser, L., Yuan, B., Karl, T., Haggerty, J., Hall, S., Ullmann, K., Smith, J., and Ortega, J., Tropospheric HONO distribution and chemistry in the southeastern US, Atmos. Chem. Phys., 18(12), 9107–9120, doi:10.5194/acp-18-9107-2018, 2018.

Zhang, L., Wang, T., Zhang, Q., Zheng, J., Xu, Z., and Lv, M.: Potential sources of nitrous acid (HONO) and their impacts on ozone: A WRF-Chem study in a polluted subtropical region, J. Geophys. Res. Atmos., 121, 3645–3662, 2016.

Zhang, N., Zhou, X., Shepson, P. B., Gao, H., Alaghmand, M., and Stirm, B.: Aircraft measurement of HONO vertical profiles over a forested region, Geophys. Res. Lett., 36, L15820, doi:10.1029/2009GL038999, 2009.